Natural Resources Canada | Ressources naturelles Canada

GEOMATICS CANADA
OPEN FILE 74

Assessment of approaches and costs associated with the correction of the HRDEM product data in the Canadian Arctic

C. Papasodoro, D. Bélanger, G. Légaré-Couture, H.A.J. Russell, and 4DM Inc.

2023

Canada

GEOMATICS CANADA
OPEN FILE 74

Assessment of approaches and costs associated with the correction of the HRDEM product data in the Canadian Arctic

C. Papasodoro[1], D. Bélanger[1], G. Légaré-Couture[1], H.A.J. Russell[2], and 4DM Inc.

[1]Canada Centre for Mapping and Earth Observation, 212 - 50 Place de la Cité, P.O. Box 162, Sherbrooke, Quebec
[2]Geological Survey of Canada, 601 Booth Street, Ottawa, Ontario

2023

Permanent link: https://doi.org/10.4095/331974

This publication is available for free download through GEOSCAN (https://geoscan.nrcan.gc.ca/).

Recommended citation

Papasodoro, C., Bélanger, D., Légaré-Couture, G., Russell, H.A.J., and 4DM Inc., 2023 Assessment of approaches and costs associated with the correction of the HRDEM product data in the Canadian Arctic; Geomatics Canada, Open File 74, 67 p. https://doi.org/10.4095/331974

Publications in this series have not been edited; they are released as submitted by the author.

ISSN 2292-7875
ISBN 978-0-660-49341-1
Catalogue No. M103-3/74-2023E-PDF

Natural Resources Canada | Ressources naturelles Canada

Canada

Assessment of approaches and costs associated with the correction of the HRDEM product data in the Canadian Arctic

Final Report

November 24, 2022

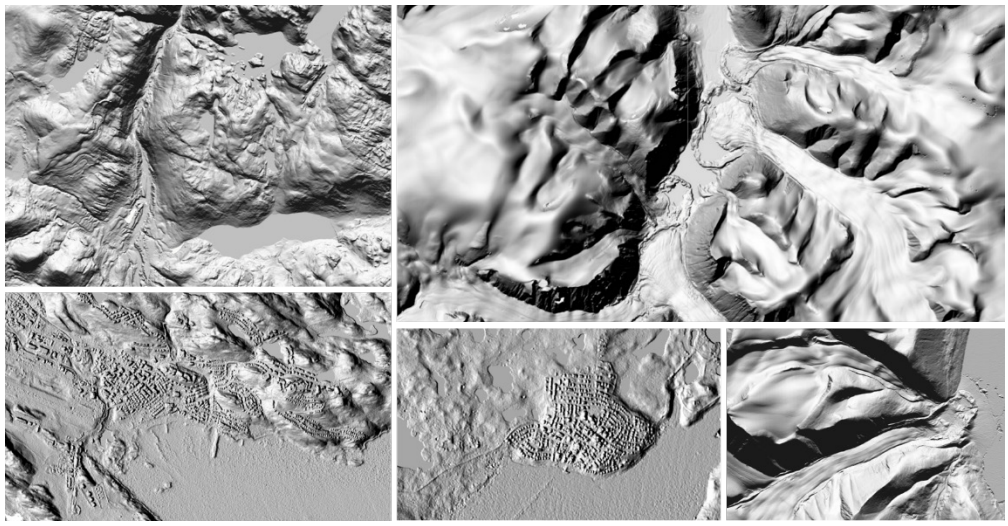

4DM

Providing solutions through mapping technology...

TABLE OF CONTENTS

TABLE OF FIGURES

TABLES

ACRONYMS

AOI	Area of Interest
ANUDEM	Australia National University Digital Elevation Model
CCMEO	Canada Centre for Mapping and Earth Observation
CGAN	Conditional Generative Adversarial Network
DEM	Digital Elevation Model
DLR	Deutsches Zentrum für Luft- und Raumfahrt, German Aerospace Center
DSM	Digital Surface Model
DTM	Digital Terrain Model
DSF	Delta Surface Fill
FGAN/FHR	(Forschungsgesellschaft für Angewandte Naturwissenschaften/Forschungsinstitut für Hochfrequenzphysik und Radartechnik, i.e., Defense Research Facility for Applied Science/Research, Institute for High-frequency Physics and Radar Techniques)
F-SAR	F-Synthetic Aperture Radar
GCP	Ground Control Points
GeoSAR	Geographic Synthetic Aperture Radar
GLISTIN-A	Glacier and Interferometric Ice Surface Topography Interferometer-Airborne
GNSS	Global Navigation Satellite System
GML	Geiger Mode LiDAR
GDEM	Global Digital Elevation Model
HRDEM	High Resolution Digital Elevation Model
InSAR	Interferometric Synthetic Aperture Radar
LiDAR	Light Detection and Ranging
MetaSAR	Meta Synthetic Aperture Radar
MiniSAR	Mini Synthetic Aperture Radar
NASA	National Aeronautical and Space Administration
NEO	NASA Earth Observation
NGA	National Geospatial Agency
NWT	Northwest Territory
NRCan	Natural Resources Canada
ONERA	Office National d'Etudes et de Recherches Aérospatiales
MODIS	Moderate Resolution Imaging Spectroradiometer
PAMIR	Phased Array Multifunctional Imaging Radar
RAMSES	Radar Aeroporte Multi-spectral d'Etude des Signatures
RCM	Radarsat Constellation Mission
RESTEC	Remote Sensing Technology Center of Japan
RPC	Rational Polynomial Coefficients
SAR	Synthetic Aperture Radar
SETSM	Surface Extraction by TIN-based Search Space Minimization
SETHI	Système Expérimental de Télédétection Hyperfréquence Imageur
SPL	Single Photon LiDAR
SRTM	Shuttle Radar Topography Mission
USGS	United State Geological Survey
WGS84	World Geodetic System 1984

ACKNOWLEDGMENTS

This report was financed through the 2021-22 GEM-GeoNorth program, led by the Geological Survey of Canada (GSC), NRCan. Following a successful proposal prepared by a joint team from the Canada Centre for Mapping and Earth Observation (CCMEO) and the GSC, a Request for Proposal was sent to the industry and a contract (#3000736431) was awarded to the company 4DM Inc. The report was prepared by 4DM Inc. between December 2021 and June 2022 and was jointly finalized with CCMEO during the fall of 2022.

INTRODUCTION

The High-Resolution Digital Elevation Model (HRDEM) was created as part of the National Elevation Data Strategy to provide detailed elevation data across the country. For the Canadian Arctic, the HRDEM was based on the ArcticDEM initiative with additional post-processing by the Canada Centre for Mapping and Earth Observation (CCMEO) to create a 2-meter Digital Surface Model (DSM) covering a geographic region of approximately 4.6 million km^2.

This report provides details on the investigation of the data issues within HRDEM, available open and commercial sources of elevation data that could be used to improve the DSM, and technologies available to generate high resolution DSM at similar levels of accuracy and resolution than the current HRDEM. In addition, the report summarizes the results of a research into the common, as well as more advanced (e.g., machine learning), methods for improving DSM.

Development of ArcticDEM has provided significant benefits in the mapping of the Canadian Arctic landscape. However, there are limitations and discrepancies in the quality of the DSM due to problems that occur in stereo-photogrammetric process, RPC errors, illumination condition/low contrast, smooth texture terrain for image matching and clouds to name a few. Although CCMEO's post-processing made considerable improvement, the DSM has voids and artifacts that are prevalent in the data. Figure 1 shows an example of data voids where satellite imagery was not obtained.

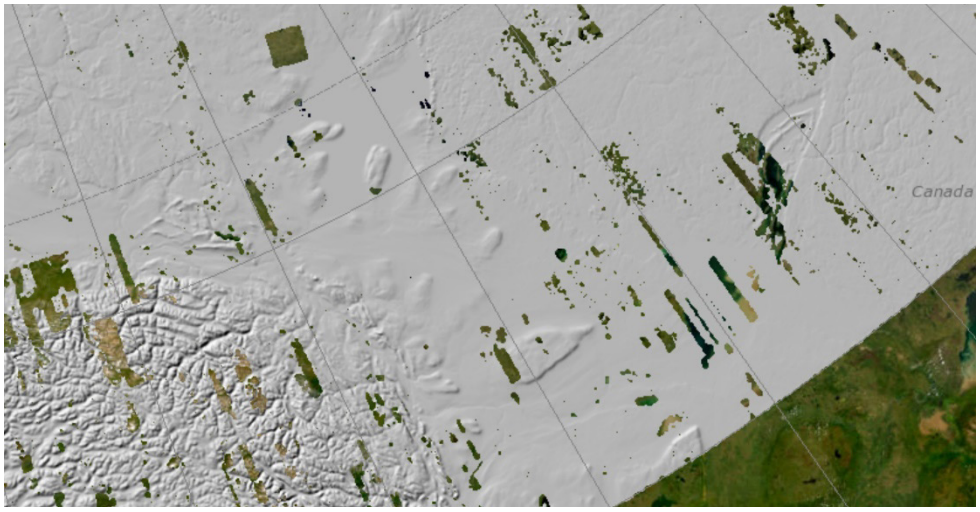

Figure 1. Data voids in ArcticDEM

Other anomalies that are persistent within the ArcticDEM include discontinuities at the land, water, and sea ice interface. An example of DSM artifacts is shown in the lower right corner of Figure 2. Artifacts are characterized by abrupt and incoherent shifts in elevations in the ArcticDEM. Data voids located over the ocean are present on the left part of Figure 2, as well as near the artifacts over the lower right corner.

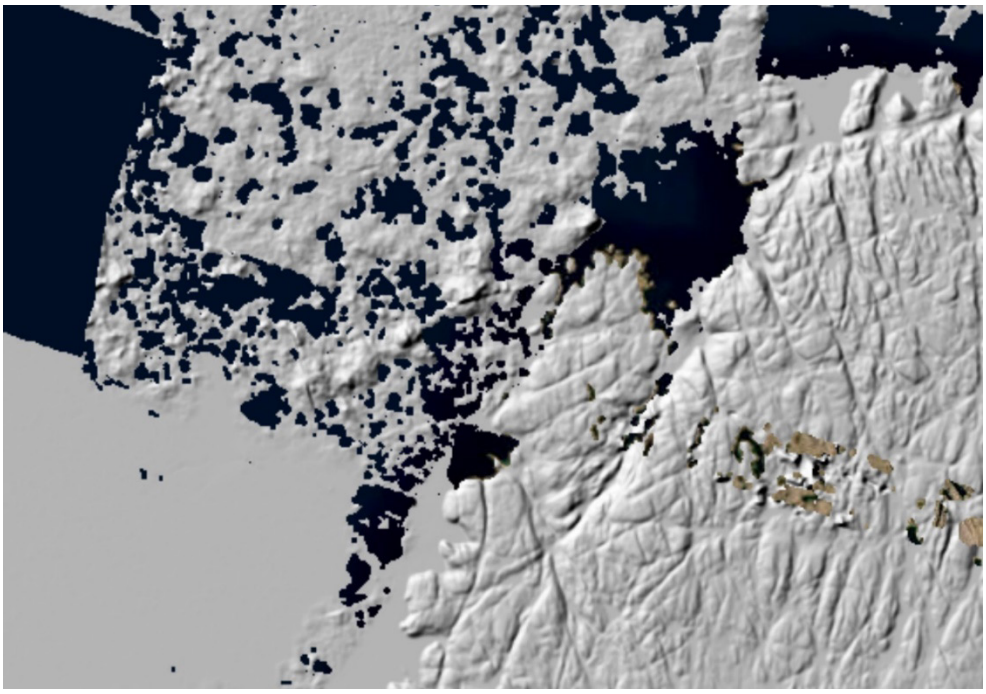

Figure 2. Example of data issues in ArcticDEM land/ocean areas

Figure 3 shows examples of elevation flattening of the DSM data within the ArcticDEM.

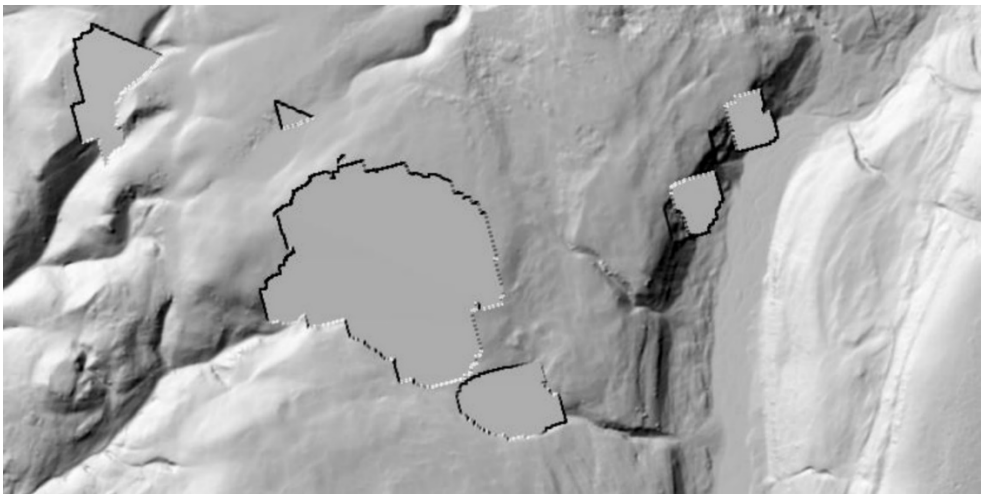

Figure 3. Flattened areas in ArcticDEM

ARCTICDEM

The ArcticDEM data product was developed through a consortium partnership involving the National Geospatial Agency (NGA) and National Science Foundation, along with universities and commercial partners. Maxar satellite imaging constellation (GeoEye-1, WorldView-1, 2, and 3) was contracted by NGA to acquire overlapping pairs of high-resolution optical imagery. A stereo autocorrelation technique was used to generate the DSM from the image pairs. ArcticDEM comes as both strip data and mosaic data in GeoTiff format using a polar stereo projection. The Canadian portion of the ArcticDEM used in developing HRDEM was part of version 3 release 7 and was considered the final release as of September 28, 2018 (Polar Geospatial Center, personal communication, 2022).

The specific method used for creating the ArcticDEM was Surface Extraction by TIN-based Search Space Minimization (SETSM). SETSM process has been used to automate the DSM creation for ArcticDEM tiles. SETSM is specifically designed for sub-meter imagery over variable terrain including snow, ice, and shadow topography (Noh and Howat, 2017).

For version 3 release 7, ArcticDEM strips represent the output from SETSM and preserve the original temporal resolution of the images. Each strip is associated with a particular acquisition date and time. ICESat altimetry data were used to improve the accuracy of the DEM by providing XYZ offsets to the strips (Polar Geospatial Center, personal communication, 2022). The mosaics were compiled from multiple strips. The process is further described in this report.

DEVELOPMENT OF THE HRDEM

The development of Canadian HRDEM for the Arctic involved the integration of ArcticDEM version 3 release 7 (Mosaics) as the base data source. Additional processing was done that included lake flattening, data voids filtering and conducting a geodetic transformation from WGS84 ellipsoidal height to the orthometric Canadian vertical datum (CGVD2013).

Lake flattening was performed using vector layers from the National Hydro Network (NHN), whereby the minimum elevation found at the edge of a lake was attributed to all the pixels located within the lake boundaries. A small number of lakes were not flattened because of discrepancies between the NHN features and the DEMs, mainly due to a too large temporal difference between the two datasets.

The handling of data voids consisted of filtering and ignoring all voids greater than 4 km^2. All voids that were less than 0.01 km^2 located outside of any hydrographic features (waterbodies, watercourses and ocean) were filled using the GDAL library - Fill No Data function which is based on an inverse distance weighting interpolation algorithm. In addition, data voids less than 0.15 km^2 touching a waterbody and not touching any land features (i.e., geological structures from the CanVec 1:50k e.g., eskers or moraines) and not representing a complete island were filled as well. The purpose of this process was the removal of many slivers around the lakes that were flattened. Voids less than 4 km^2 and completely included within watercourses were also filled. Areas of high roughness determined by GDAL's TRI algorithm over watercourses (based on NHN 1:50K) were converted to voids.

The remaining void areas along lakes were filled by interpolating from valid pixels around these areas. However, uncorrected anomalies remain over land and ocean, particularly along void areas.

During the validation process, the most obvious and noticeable remaining artifacts were identified and vectorized by CCMEO technicians. These polygon vectors are disseminated with the HRDEM product and are intended to guide the user with regards to areas where the product if of less quality.

Furthermore, oceans further than 1 km from the inland were converted to voids.

Overall, the processing applied to ArcticDEM during the integration into the HRDEM has greatly improved the product, although problems still remain.

THE PATH FORWARDS

The intent of this investigation was to provide supporting information to address the data anomalies in HRDEM and present a path forward. Data anomaly used in this report consists of a combination of data artifacts and data voids.

Research and analysis were conducted to identify the characteristics of data anomalies in HRDEM, available open source and commercial sources of elevation data to improve HRDEM, as well as accessibility of satellite and airborne remote sensing technology applicable for collecting new data to eliminate the anomalies. In addition, methodology and processes were investigated to integrate the new elevation data to improve the quality of HRDEM.

ArcticDEM data source limitations and process issues produce anomalies that were inherited by HRDEM. The anomalies are mainly located over low contrast areas like snow-covered areas and water and shorelines (land/water interface). Furthermore, areas with patterned textures like forests were also problematic. Finally, discontinuous surfaces like cliffs make photogrammetric matching difficult. All these areas impair the performance of the feature matching algorithm that relies on high contrast, continuous and unambiguous surface textures. Furthermore, the geolocation accuracy provided by the satellite sensors using rational polynomial coefficients (RPCs) may result in an offset between corresponding features in the stereo pairs and thus negatively impact feature matching. In the case of void areas, environmental conditions such as clouds, fog, and shadows, can prevent high-quality elevation data from being obtained.

Even after improvements to HRDEM, there are over 48,583 anomalies in the data, totalling over 111,338 km^2 or approximately 2% of HRDEM. The total area of anomalies is relatively small considering the scale of the Arctic, however, the distribution and location of data anomalies can impact the confidence in using the data.

To create the path forwards on improving HRDEM, the next section presents an analysis of the data anomalies. The information is used to determine solutions to best resolve the data issues.

CANADIAN HRDEM ANOMALIES

A detailed analysis of HRDEM anomalies was conducted to assess the magnitude and distribution of data voids and artifacts by tiles. Specifically, anomalies were quantified by their number and area within a given tile. CCMEO provided a shapefile of the location of the data anomalies. The analysis also examined potential associations between data voids and generalized land cover types, and elevation. Cloud condition analysis was also conducted as data was acquired using optical satellite images. The purpose of the analysis was to determine the magnitude, characteristics, and distribution pattern of the anomalies to guide the appropriate technology, data source and methods needed to correct HRDEM.

DATA VOIDS

Data void analysis was conducted to compile the number and area of data voids by tiles. Figure 4 and Figure 5 show void counts and percentages by tiles. Approximately 64% of tiles have between 1 and 20

data voids of any size within a tile of 50 km x 50 km. It should be noted that tiles can have multiple voids of different area size within a single tile and therefore can be counted in different area ranges.

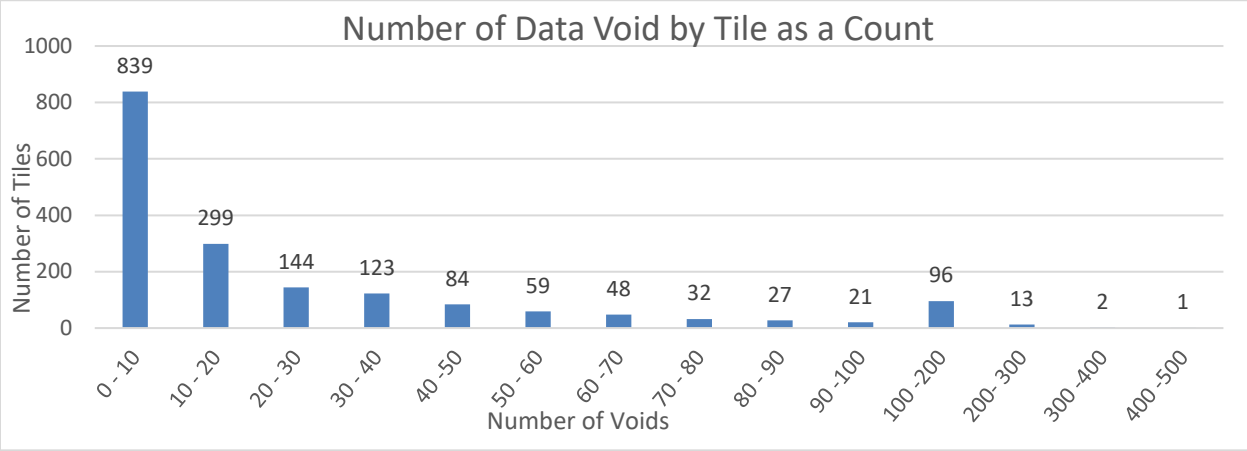

Figure 4. Tiles with data voids by counts

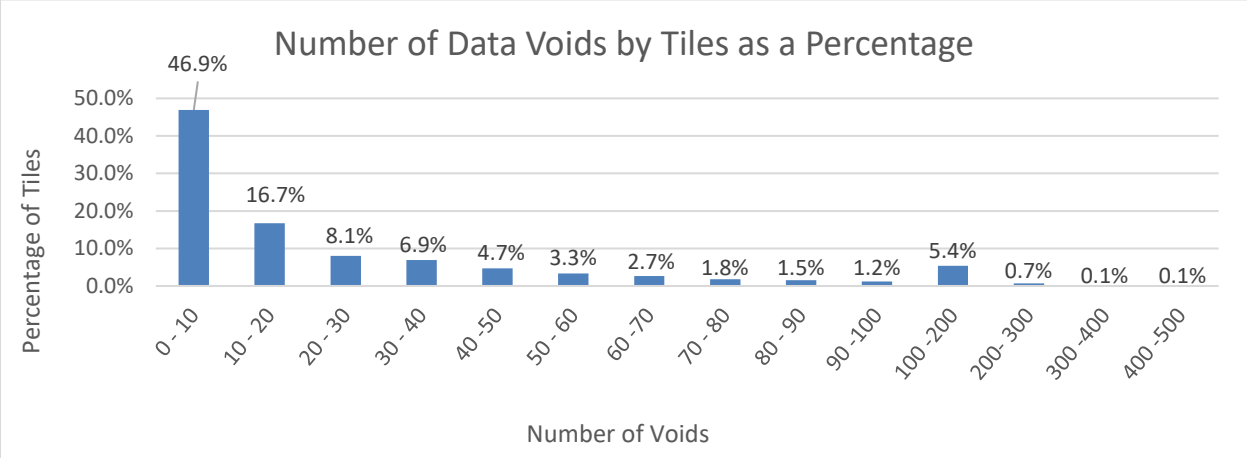

Figure 5. Tiles with data void by percentage

Figure 6 and Figure 7 illustrate the distribution of data void area by tile. 63% of void areas are within the 0–6 km^2 range.

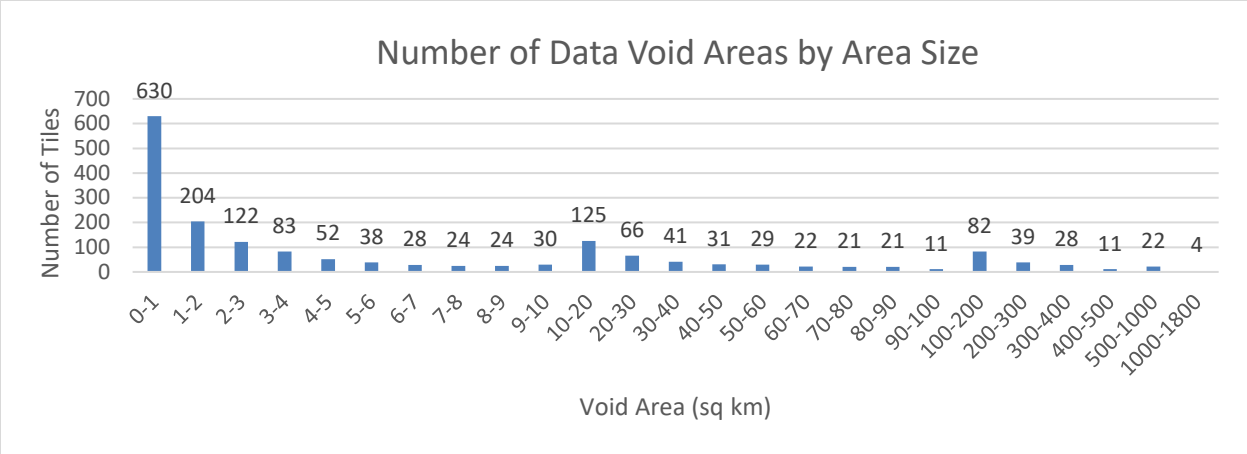

Figure 6. Area of data voids by tiles as counts

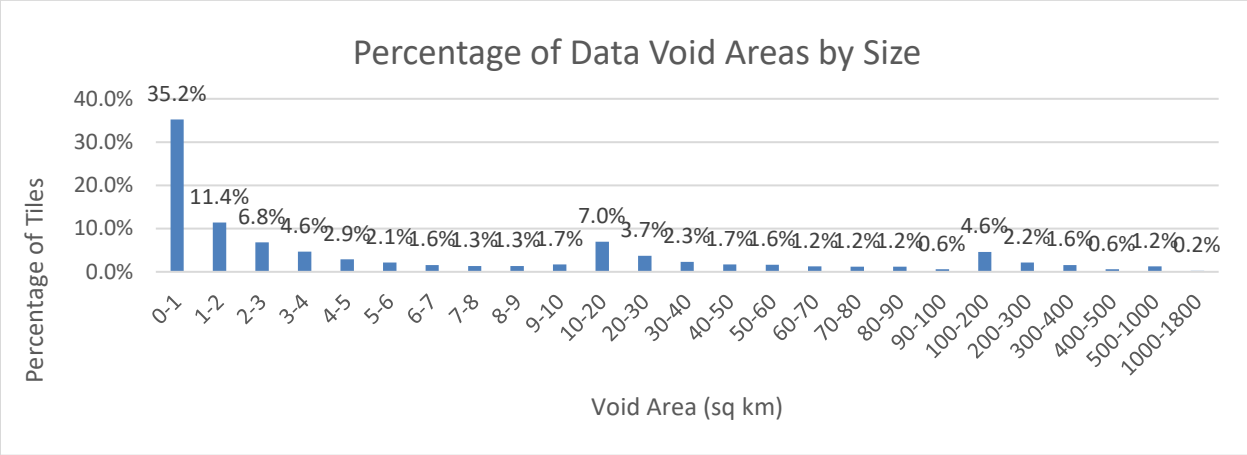

Figure 7. Area of data voids by tiles as a percentage

A map of the data void areas was produced to illustrate the geographic distribution within the HRDEM area. Figure 8 reveals that the distribution of data voids is non-uniform. The map shows a concentration of data voids in the Yukon area that corresponds to mountainous terrain and forested area. Another notable location is the glaciated areas in the Canadian Arctic Archipelago, showing clustering of data voids.

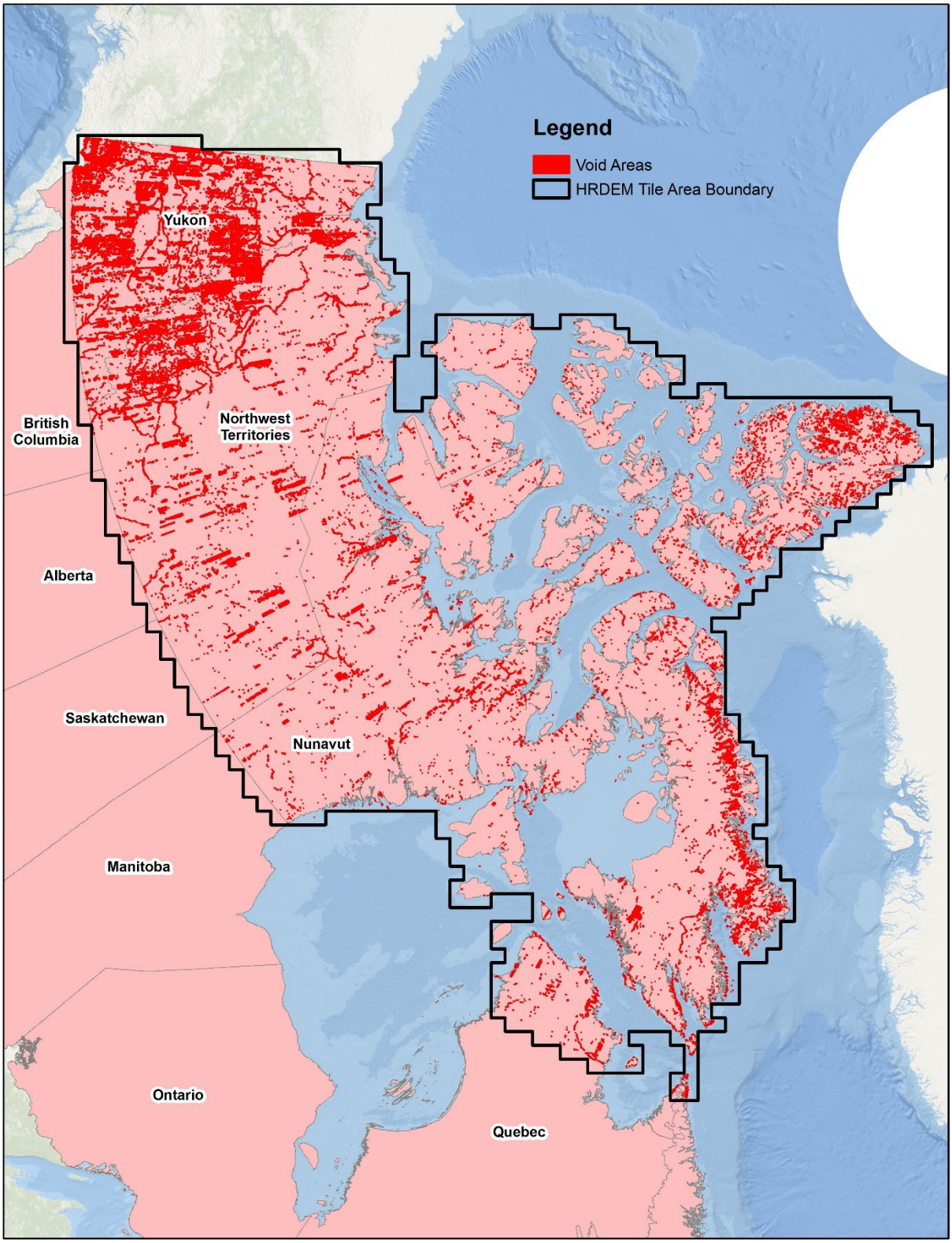

Figure 8. Distribution of data void area in HRDEM

DATA ARTIFACTS

The distribution of artifacts in HRDEM was also investigated. The artifacts were identified and mapped by CCMEO technicians selecting the most obvious and noticeable artifacts. It should be noted that not all deficiencies have been identified and mapped in HRDEM. Figure 9 and Figure 10 show the distribution of artifacts by tiles by counts and percentages. The distribution of artifacts by tiles indicates that most tiles (about 79%) have between 1 and 10 artifacts.

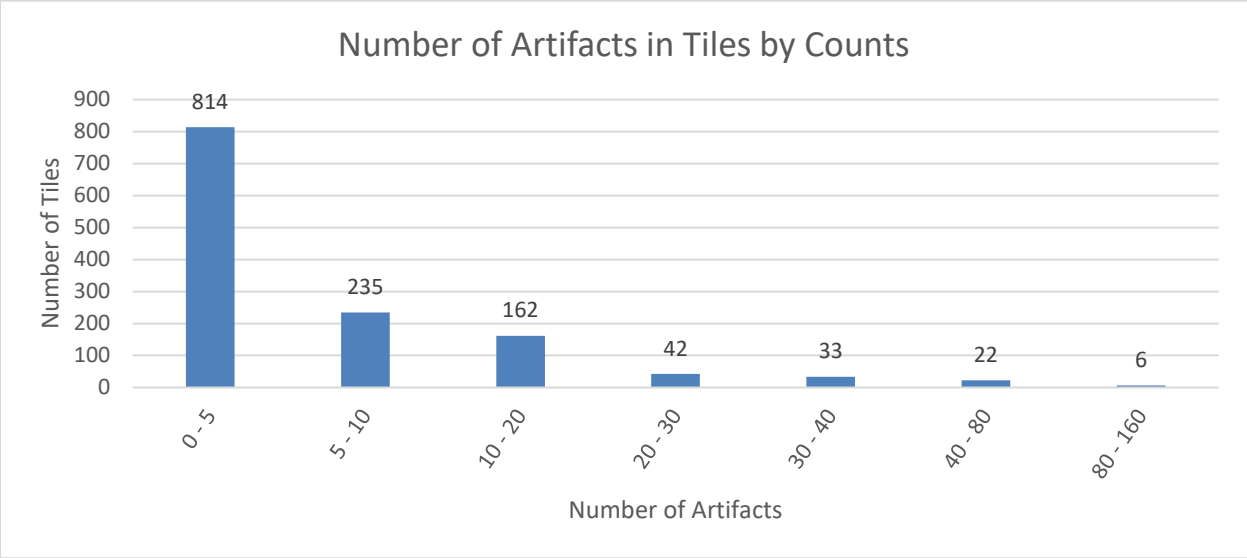

Figure 9. Number of tiles with artifacts by counts

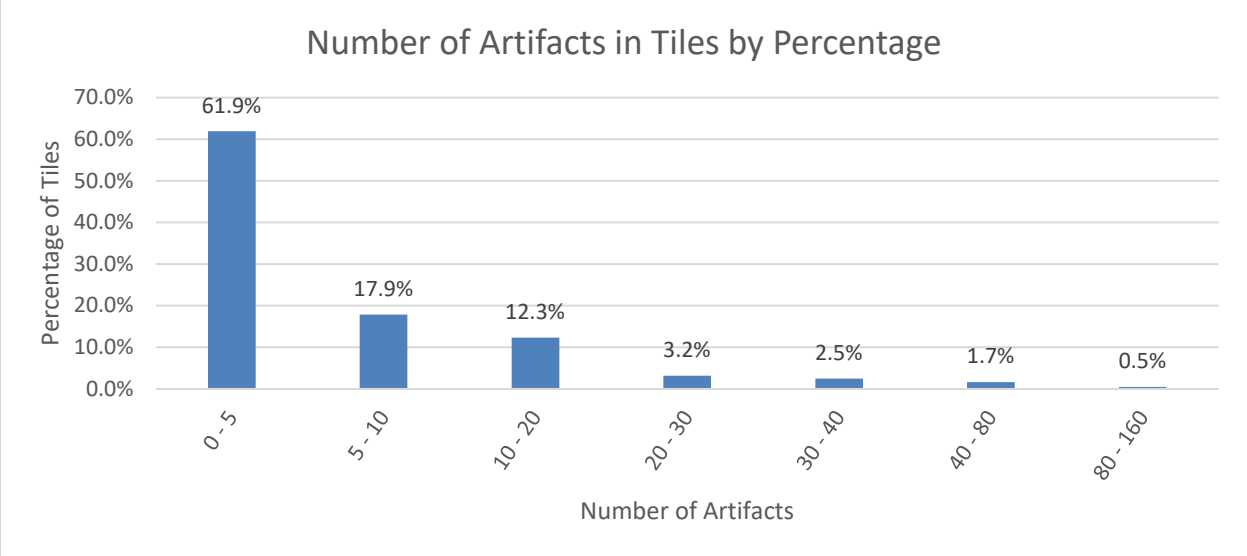

Figure 10. Number of tiles with artifacts by a percentage

An area calculation was conducted for the artifacts by tiles and percentage and is shown in Figure 11 and Figure 12. Approximately 44% of tiles have artifacts areas in the 1–6 km^2 range, while about 8% have artifacts covering more than 100 km^2.

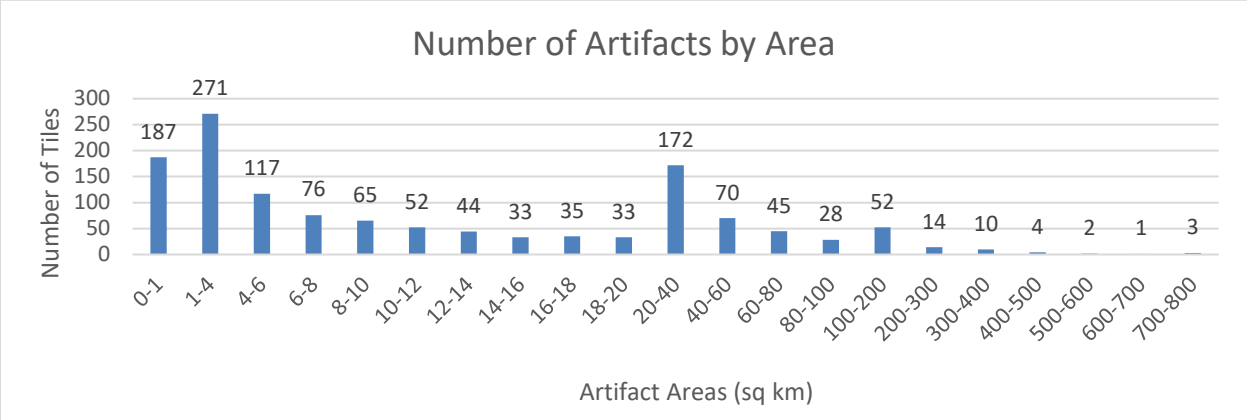

Figure 11. Number of tiles by area of artifacts by counts

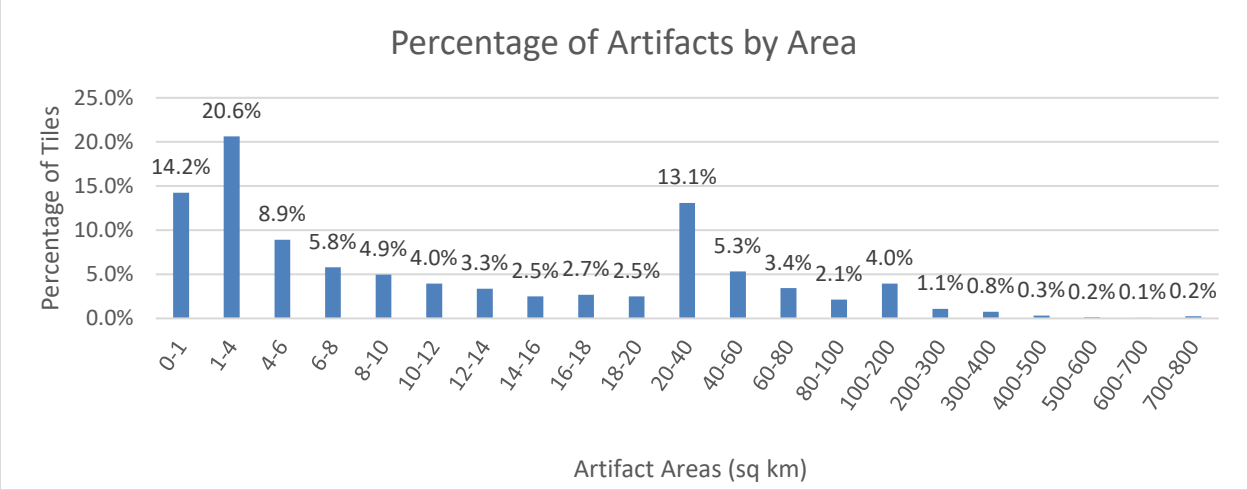

Figure 12. Number of tiles by area of artifacts by a percentage

The map in Figure 13 shows the geographic distribution of artifacts across the HRDEM in the Canadian Arctic.

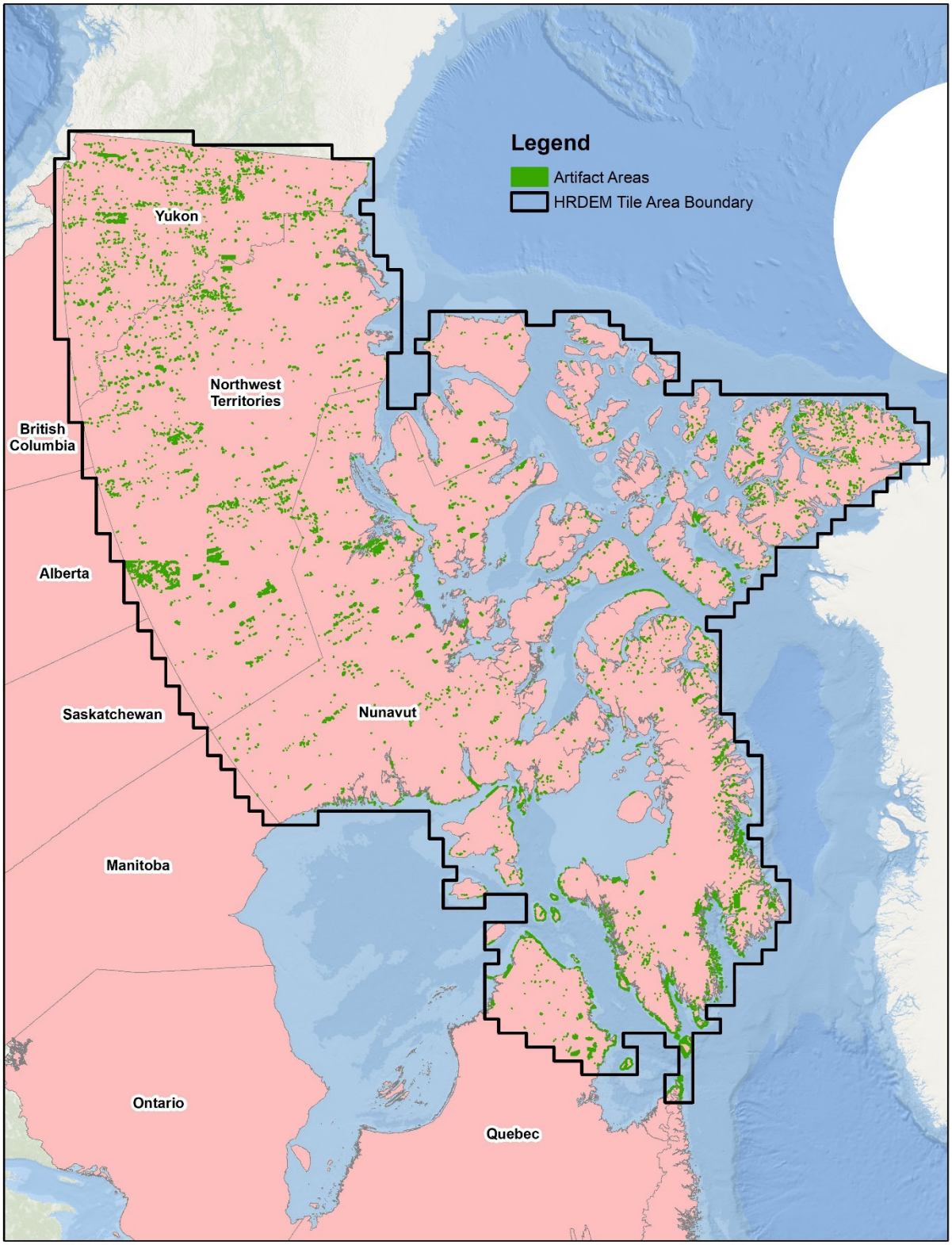

Figure 13 HRDEM Artifact Map

DATA ANOMALIES

HRDEM anomalies of both kinds (artifacts and voids) were tabulated. Figure 14 shows the distribution of data anomalies by tile as a percentage. 50% of data anomalies are smaller than 10 km^2, 35% are between 10 and 100 km^2, and another 15% are larger than 100 km^2.

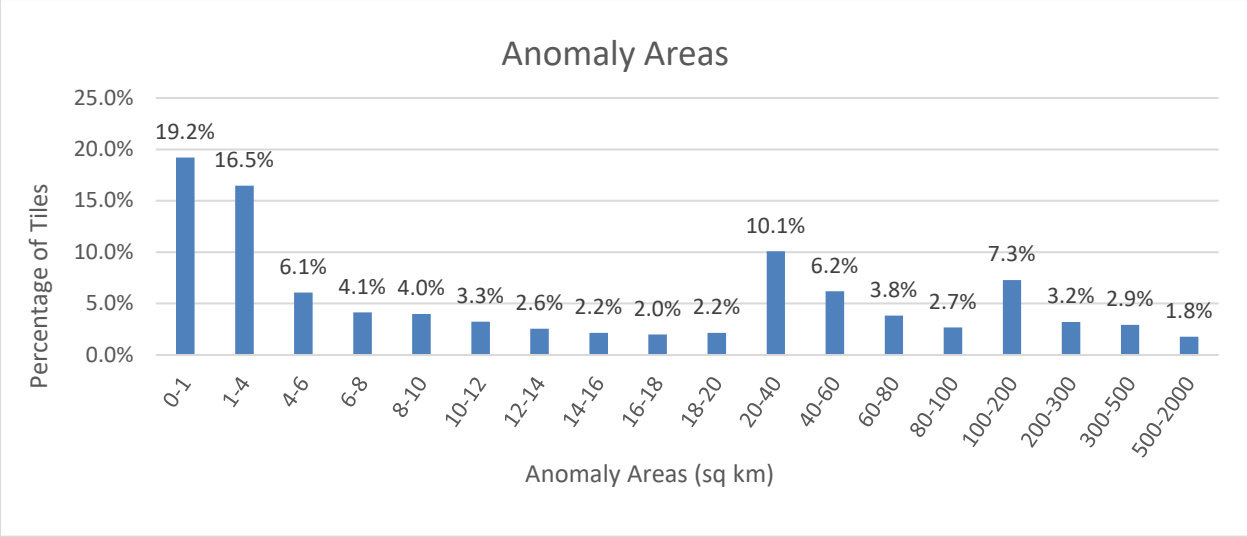

Figure 14. Percentage by tile with anomalies by area

Table 1 providing a summary of the anomalies in HRDEM is presented. Overall, 88% of the tiles have anomalies, while 12% of tiles no data issues were detected in the data provided by CCMEO. It should be noted that unaccounted data anomalies may exist and were not part of this analysis. Data voids are the predominant type of data anomaly, with 82% of tiles having a void area. The largest combined artifact and void area is 1,958 km^2 in a single tile or 78% of the tile.

Table 1. Summary of anomalies (voids and artifacts)

Description	Tile Count	Percentage
Number of tiles with no issues	260	12%
Number of tiles with anomalies	1910	88%
Number of tiles with voids	1788	82%
Number of tiles with artifacts	1340	62%

Total number of tiles in HRDEM **2170**

A composite map of HRDEM anomalies by tile was created in Figure 15. The map shows the locations of both kinds of data anomalies, as well as the tiles without anomalies.

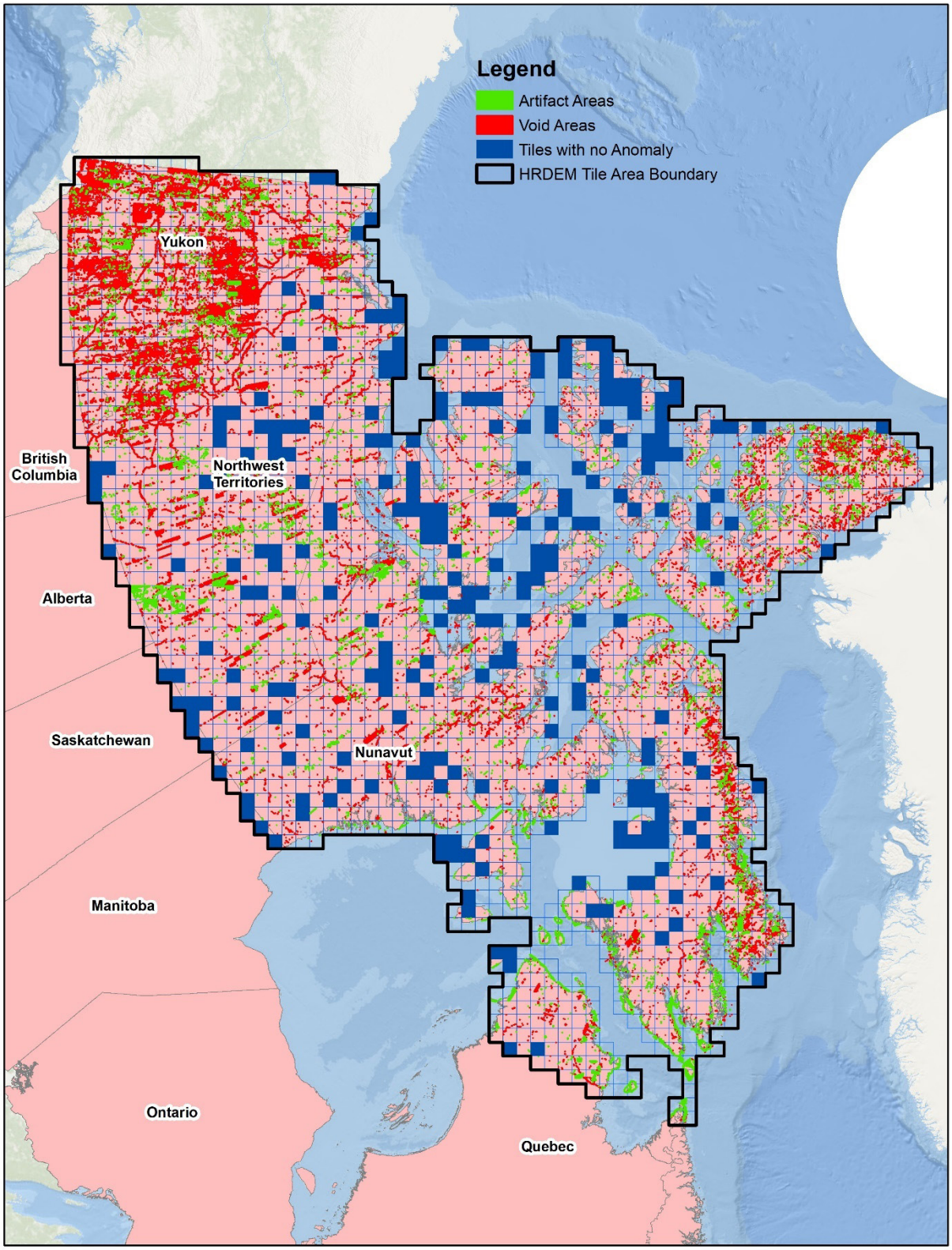

Figure 15. HRDEM Tiles with Anomalies

LAND COVER ANALYSIS

A geospatial zonal analysis was conducted to determine the predominant land cover type(s) associated with data anomaly areas. The 2015 Land Cover of Canada digital map at 30 m resolution[1] was used as the reference source. The analysis was tabulated by the 15 land cover classes.

Data Artifacts

An overlay of data artifact was conducted with land cover map. The purpose of this analysis was to provide information to guide suitable data and methodology for correcting the issues. Figure 16 shows an example of the artifact polygons associated with land cover classes.

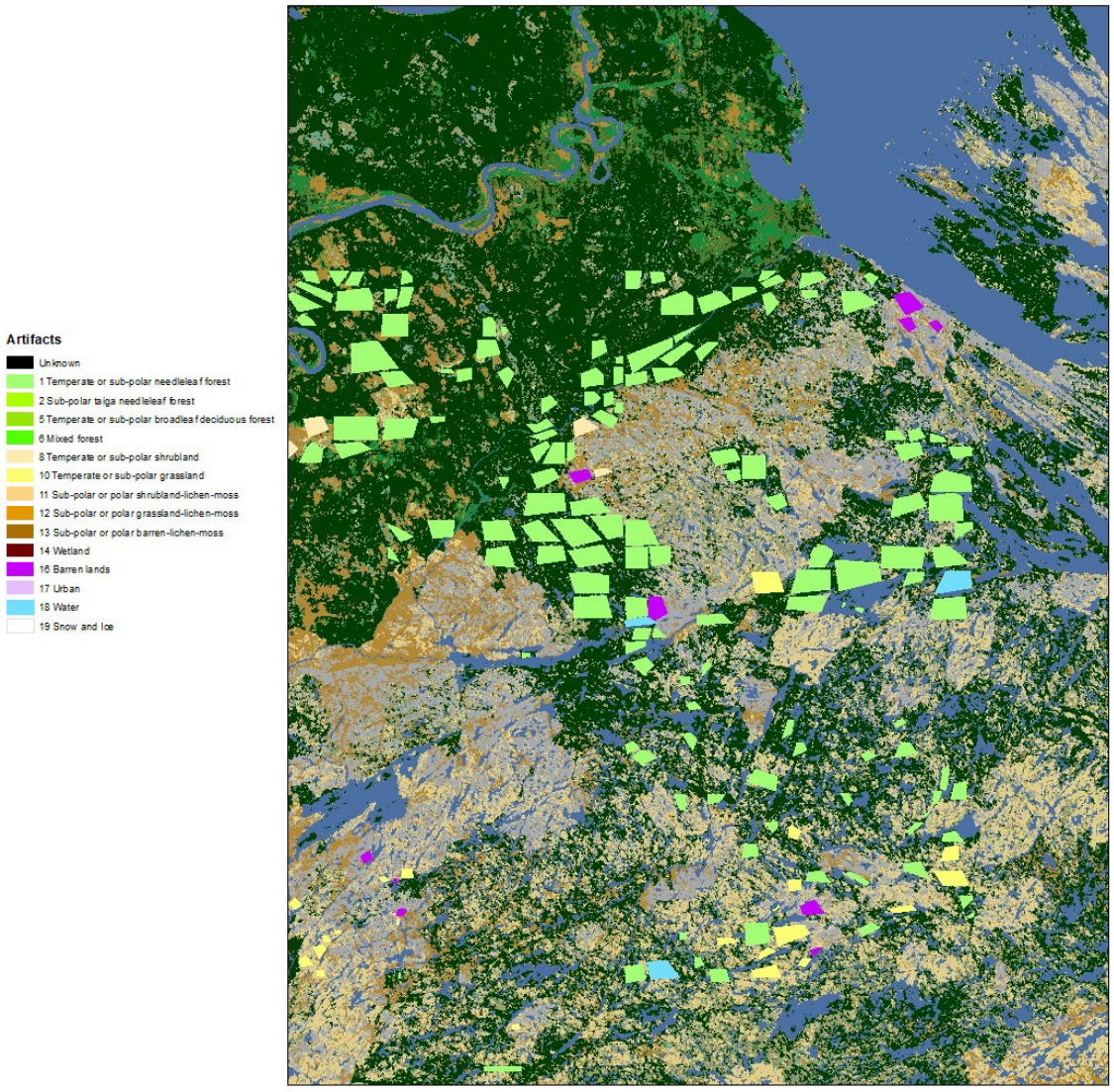

Figure 16. Data artifacts and land cover classes

A summary of land cover type associated with data artifacts is provided in Table 2 below.

Table 2. Summary of data artifacts by land cover classes

Landcover Classes	Areas	Area (sq km)

[1] https://open.canada.ca/data/en/dataset/4e615eae-b90c-420b-adee-2ca35896caf6

Unknown	1.1%	425
Temperate or sub-polar needleleaf forest	14.7%	5,785
Temperate or sub-polar broadleaf deciduous forest	0.8%	330
Sub-polar taiga needleleaf forest	0.0%	13
Mixed forest	0.3%	98
Temperate or sub-polar shrubland	1.5%	603
Temperate or sub-polar grassland	3.2%	1,245
Sub-polar or polar shrubland-lichen-moss	1.8%	720
Sub-polar or polar grassland-lichen-moss	12.2%	4,804
Sub-polar or polar barren-lichen-moss	6.1%	2,383
Wetland	0.1%	44
Barren lands	13.6%	5,363
Urban and Buildup	0.0%	0
Water	37.4%	14,706
Snow and Ice	7.2%	2,834
	100%	39,355

The results show that water, coniferous forests, barren lands, and grassland-lichen-moss make up 78% of the area associated with artifacts.

Data Voids

An overlay of data voids was also conducted with the land cover map for similar purpose as explain for data artifacts. Figure 17 shows an example of the void polygons with land cover classes.

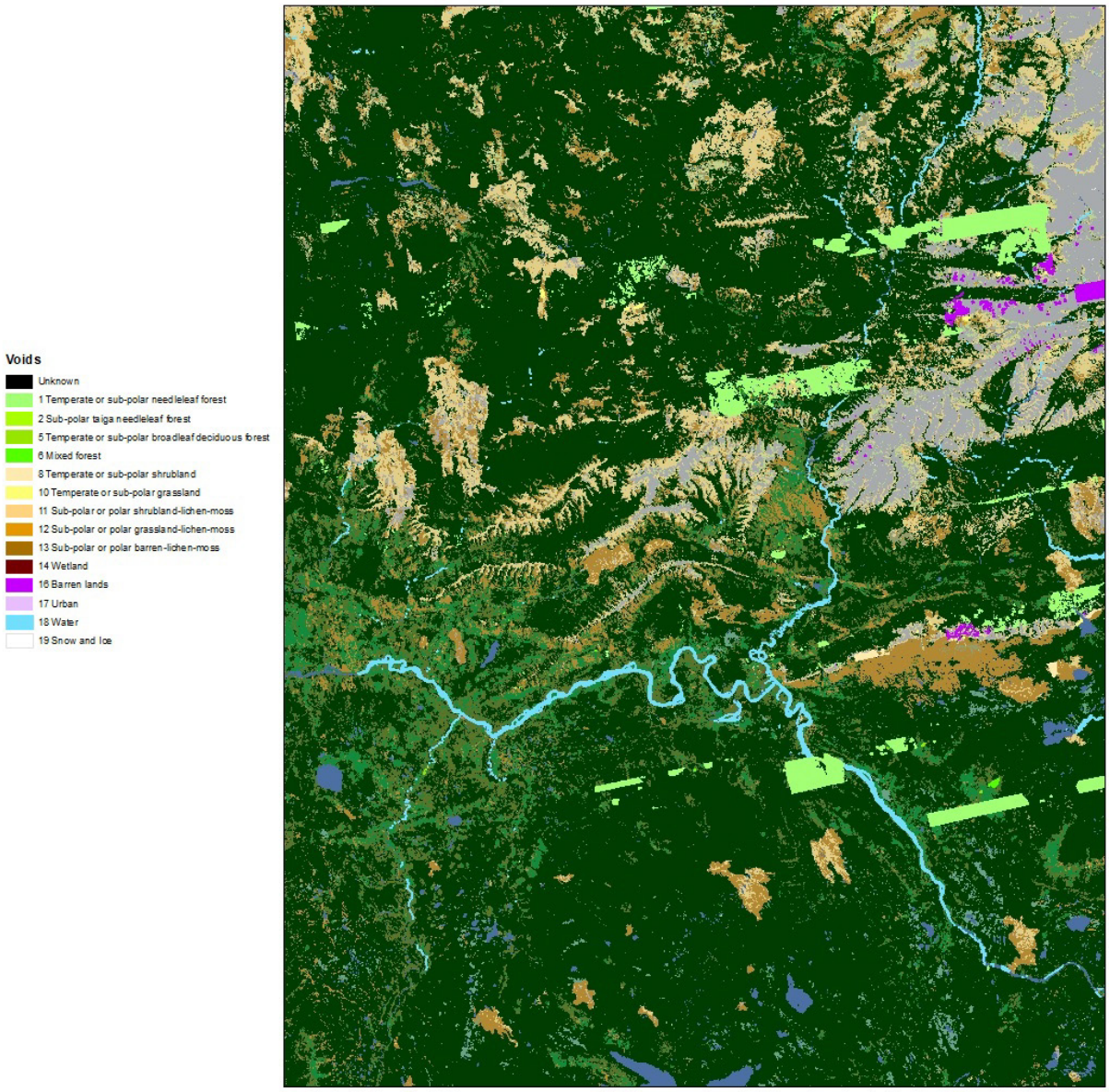

Figure 17. Data voids and land cover classes

A summary of data voids by land cover type is provided in Table 3 below.

Table 3 Summary of data voids by land cover classes

Landcover Classes	Area	Area (sq km)
Unknown	0%	8
Temperate or sub-polar needleleaf forest	37%	26,636
Temperate or sub-polar broadleaf deciduous forest	1%	441
Sub-polar taiga needleleaf forest	0%	50
Mixed forest	0%	247
Temperate or sub-polar shrubland	5%	3,282
Temperate or sub-polar grassland	4%	2,792

Sub-polar or polar shrubland-lichen-moss	2%	1,557
Sub-polar or polar grassland-lichen-moss	9%	6,771
Sub-polar or polar barren-lichen-moss	2%	1,244
Wetland	0%	134
Barren lands	24%	17,049
Urban and Buildup	0%	6
Water	10%	7,311
Snow and Ice	6%	4,456
	100%	71,983

Like data artifacts, the results for voids show that water, coniferous forests, grassland-lichen-moss and barren lands make up 80% of the data void areas.

Data Anomalies

A combined analysis of data voids and artifacts by land cover is provided in Table 4.

Table 4. Summary of data anomalies by land cover classes

Landcover Classes	Areas	Area (sq km)
Unknown	1%	433
Temperate or sub-polar needleleaf forest	26%	32,421
Temperate or sub-polar broadleaf deciduous forest	1%	772
Sub-polar taiga needleleaf forest	0%	63
Mixed forest	0%	346
Temperate or sub-polar shrubland	3%	3,885
Temperate or sub-polar grassland	4%	4,037
Sub-polar or polar shrubland-lichen-moss	2%	2,278
Sub-polar or polar grassland-lichen-moss	11%	11,575
Sub-polar or polar barren-lichen-moss	4%	3,626
Wetland	0%	178
Barren lands	19%	22,412
Urban and Buildup	0%	6
Water	24%	22,017
Snow and Ice	7%	7,290
	100%	111,338

Overall, the top four land cover types associated with data anomalies are water, coniferous forests, polar grassland-lichen-moss and barren lands, which collectively account for 80% of the total area of data anomalies.

Visual Anomaly Distribution

A visual interpretation analysis was conducted using Google Earth. The data artifact and void polygons were merged and dissolved into anomaly polygon regions. Data was converted to a KMZ file and loaded into Google Earth for visual interpretation.

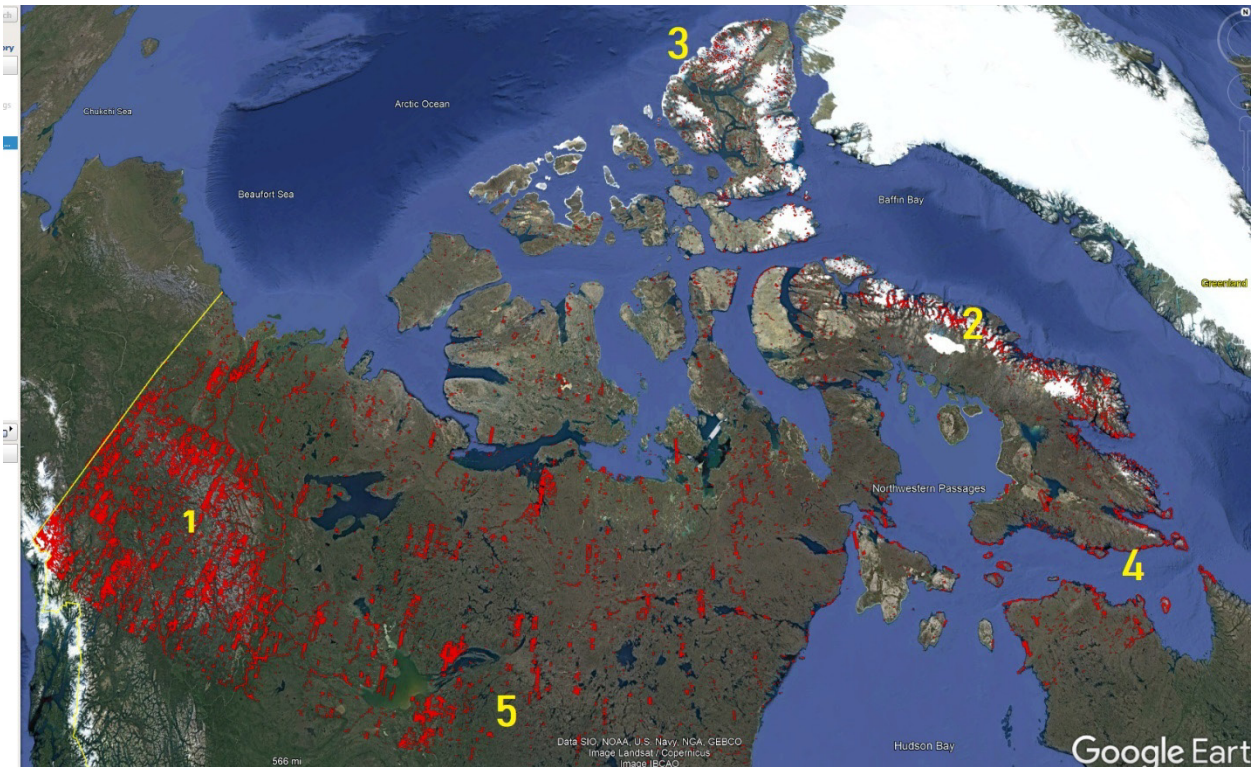

Figure 18. Distribution anomalies by elevation and glacial areas

Figure 18 shows the distribution of HRDEM anomalies. Observation of anomaly areas show concentration of anomalies in five types of locations:

1. Mountains/coniferous forests in Yukon has a high degree of clustering of data anomalies due to terrain
2. Permanent glacial/high relief area on Baffin Island has a concentration of data anomalies
3. Permanent glacial/high relief area on Ellesmere Island also has similar concentration of data anomalies
4. Sea/land anomalies around many coastlines area has anomalies likely due to the presence of sea ice during the data collection period
5. Inland waterbodies areas in the interior where elevation extraction is problematic on smooth flat surfaces.

The distribution is an important consideration for elevation data technology selection to address the deficiencies in the HRDEM.

Clouds

A macroscale cloud analysis was conducted to examine the impact on potential new data collection based on optical and LiDAR technologies in the Canadian Arctic. NASA Earth Observation (NEO) web site provides access to cloud fraction data from MODIS (Terra/Aqua) as daily, 8 days and 1-month averages. The highest spatial resolution data access is provided at 0.1-degree resolution, covering historical period of 22 years. For the cloud analysis, 2021 data was downloaded from NEO site for the months of July, August, and September. The selected period coincides to best data acquisition period due to sufficient solar elevation, irradiance, and least ground snow coverage. Figure 19 shows the July 2021 cloud fraction over the HRDEM area from MODIS.

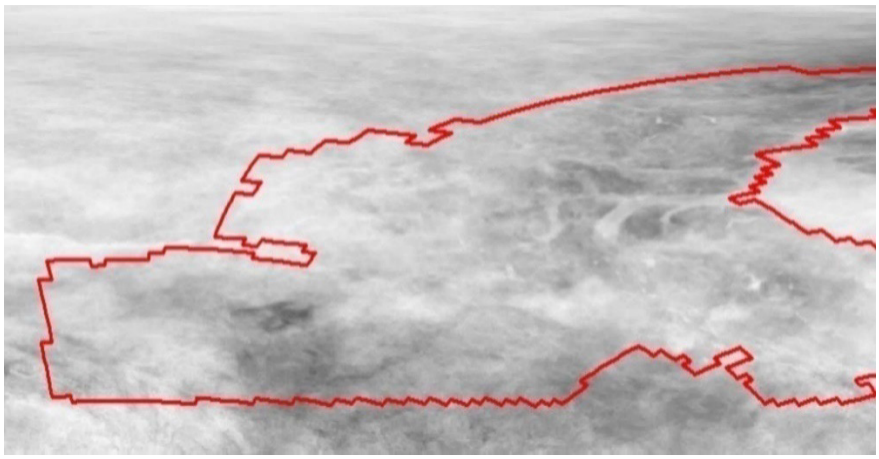

Figure 19. MODIS Cloud Fraction for July 2021 within the HRDEM

The maximum, mean, minimum and standard deviation (STDEV) for cloud fraction is shown in Table 5 for the three months. Cloud fraction is derived from the 1-km-pixel resolution cloud mask product made from radiance and reflectance measurements of Earth collected by MODIS. The cloud fraction is based on the MODIS Cloud Mask product. The algorithm employs a series of visible and infrared thresholds and consistency tests to specify confidence that an unobstructed view of the Earth's surface is observed (NASA Earth Observation-NEO Cloud Fraction). A cloud fraction of one means the pixel is completely covered with clouds, while a cloud fraction of zero represents a total cloud-free pixel.

Table 5 Cloud Fraction Estimate July, August and September 2021 in the Canadian Arctic

Cloud Fraction 2021	Maximum	Mean	Minimum	STDEV
The average cloud fraction for July:	0.98	0.72	0.27	0.1
The average cloud fraction for Aug:	0.99	0.76	0.37	0.1
The average cloud fraction for Sept:	1	0.77	0.41	0.1

The results of the cloud analysis indicated that over the summer period where snow on the ground would be at a minimum, the mean cloud fraction for each pixel over the entire Canadian Arctic region is typically high at about 0.75. In addition, clouds are present during summer time with the minimum average cloud fraction of 0.35 over July, August and September for the entire Canadian Arctic region. The information indicates the collection of optical data would need to be well planned to find suitable acquisition windows. For instance, July is more suitable month for optical imagery data collection then August and September. It should be noted that the analysis is not comprehensive, only consider one season and is across a large geographic extent. The cloud fraction values are based on MODIS observation which is not continuous, so cloud-free periods are likely. The intent of this analysis is to provide some insight into the challenge in collecting optical data in the Arctic. The results indicate that clouds present a major, but not insurmountable challenge in collecting optical data in the Arctic region.

SUMMARY OF FINDINGS

The review of HRDEM anomalies in the Canadian Arctic presented reveals that the majority of tiles (88%) have defects. In the tile analysis, 50% of these anomalies are small areas of less than 10 km^2. The largest contiguous data void area is 4,871 km^2, and the largest artifact area is 723 km^2 (Figure 20).

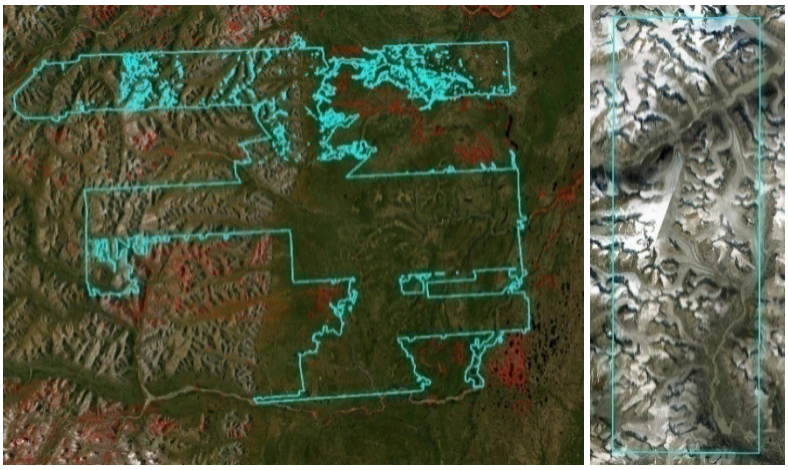

Figure 20. Large contiguous voids (left) and artifact (right) areas

The anomaly distribution in HRDEM can be associated with conifer forest, water, grassland-lichen-moss, and barren lands making up 80% of data anomalies. The combination of high relief areas and forest areas in the Yukon show a high concentration of anomalies due to landscape complexity. Glacial areas, high-relief areas, shorelines and waterbodies in the Arctic Archipelago have high concentrations of anomalies. A total known anomaly area of 111,338 km^2 is present in HRDEM or about 2% of HRDEM.

Cloud cover in the Arctic region is a challenge when considering technology for data collection. Cloud fraction analysis reveals average of 0.72 and greater (i.e., on average, pixels in the Arctic are covered by cloud about 3/4 of the time) during the months of July, August, and September which typically present the optimal period for optical imagery and LiDAR collection. During this period, solar elevations are highest and snow present on the ground is minimal.

Addressing anomalies in HRDEM would need to consider the following factors:

- Size of anomaly: small data anomalies can be addressed by applying data filling techniques, while larger require data collection or integration of existing high resolution DEM products.
- Type of anomaly: depending on if the issue is a data void, depression, disjoint seam, or shoreline issue, will affect the choice of correction measure to be applied.
- Landscape characteristics: optical stereo imagery has limitations over glacial area and high relief topography, forests, and barren area; while alternative methods would likely be more successful.
- Location: some technologies such as airborne sensors may have limitations in flying in remote location in the Canadian Arctic due to insufficient ground facilities and may not be suitable.
- Cloud cover: optical sensors are particularly affected by clouds. Other remote sensing technologies like radar are less influenced by this factor and could represent a better solution for some areas where clouds are persistent.

In the next section, the solutions to problems are investigated and reported.

SOLUTIONS

The understanding of the data anomaly attributes from the data analysis conducted in the previous section can be used to guide the solution for improving the HRDEM. Several considerations listed below are required to determine appropriate solutions to the HRDEM data anomalies.

Landscape	The topography and land cover suitable for generating DSM with the selected technology
Surface Conditions	Surface state in terms of snow cover, glacial, sea ice, water bodies
Data Availability and Licensing	Existing data in the region with similar or better resolution and accuracy with open license for public distribution
Acquisition Technology	Satellite and airborne technology suitable for elevation extraction considering surface conditions, clouds and landscape
Logistical and Risks	Limitations and restrictions to apply the acquisition technology to collect data with a reasonable time frame
Financial	Cost implications for selected technology and data sources

Improvements to HRDEM will require a combination of using existing elevation data, acquiring new data collection, and applying methods to remove the anomalies. Existing elevation data sources have been compiled and are presented as a potential DSM solution for HRDEM based on existing data.

ELEVATION DATA SOURCES

Existing commercial and open-source elevation data sources are listed in this section. Data sources have been organized by DEM spatial resolution. Investigation identifies DSM/DTM[2] data with spatial resolution of 0.5 m to 30 m data. Although higher resolution DEMs and technologies will likely be favoured for any subsequent corrections on the HRDEM, medium and lower resolution DEMs are also presented in this section to provide a more complete overview of potential solutions.

[2] In this report, a DSM contains elevations above surface features (e.g. vegetation, buildings), while a DTM contains ground elevations. The term DEM includes both DSM and DTM.

High Resolution DEM (<= 2 m)

ArcticDEM

Additional data processing is currently underway by the Polar Geospatial Center to create version 4 of the ArcticDEM. The process is using all strip data and extracting a median value. The median-based blending strategy, which was not used in version 3, release 7, will be able to make use of all valid pixels, even in a previously discarded strip. This will make more data available and reduce the number of voids encountered. The outcome is expected to provide a considerable improvement to the quality of the ArcticDEM and can be used to improve HRDEM.

To identify potential improvement areas, the ArcticDEM v3 release 7 strip coverage file from the Polar Geospatial Center was used to conduct a spatial analysis. The HRDEM data anomalies (artifacts and voids) were overlaid on ArcticDEM v3 release 7 strip data to indicate the strip locations where there is potential data improvement in the HRDEM data from the reprocessing to create ArcticDEM v4. Figure 21 shows the strip data location within the HRDEM domain. A total of 2,661 km^2 where data anomaly has no strip data, which is represented in red in the Figure 21.

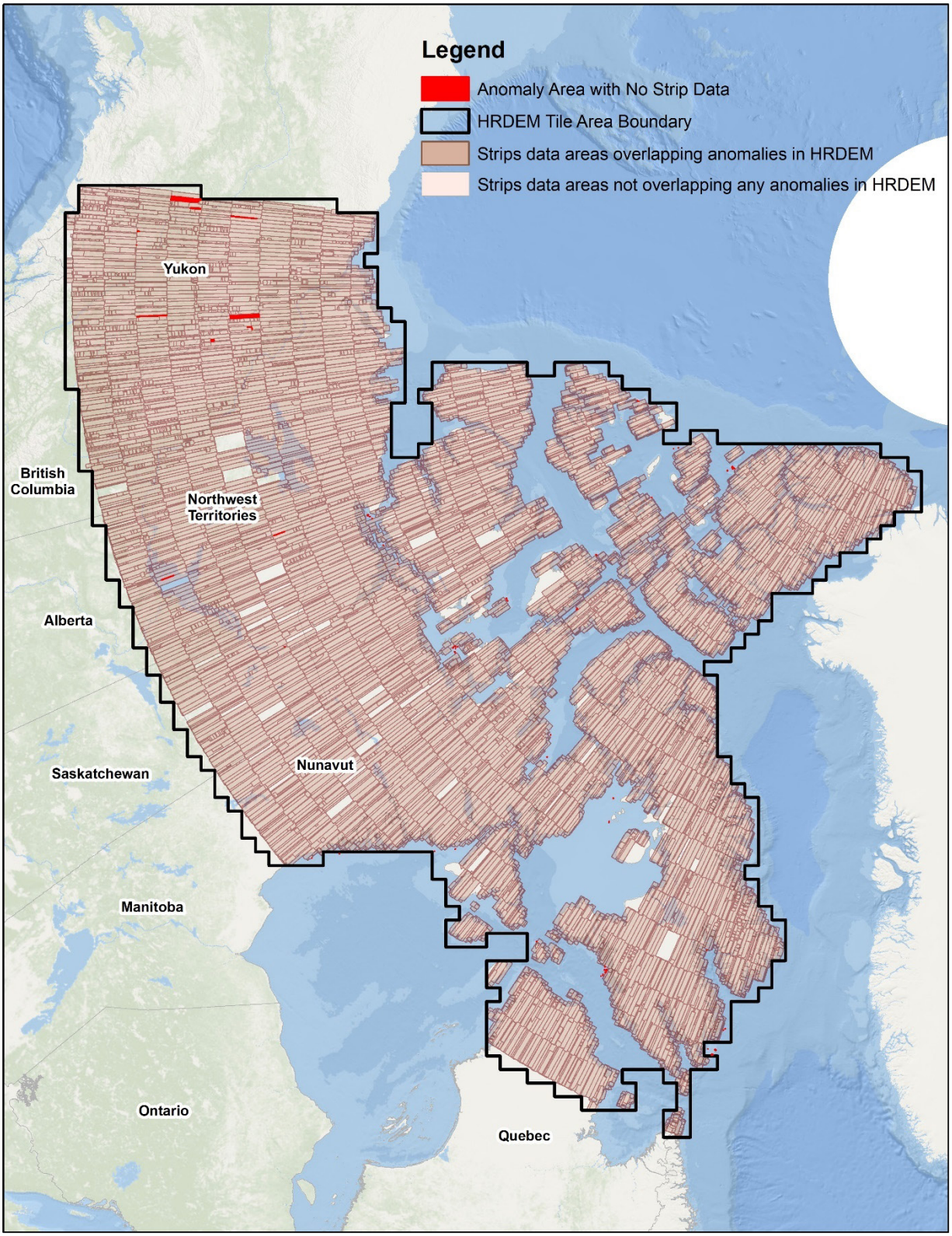

Figure 21. Strip data coverage over anomalies with the HRDEM coverage based on ArcticDEM v3 release 7

A density strip map with data anomalies overlaid on ArcticDEM v3 release 7 strip location is shown in Figure 22. The map shows locations where strip concentration is the highest to lowest. Higher overlap areas will likely see improvements to HRDEM. A new version is expected in the near future, depending on computing resources (Polar Geospatial Center, personal communication, 2022).

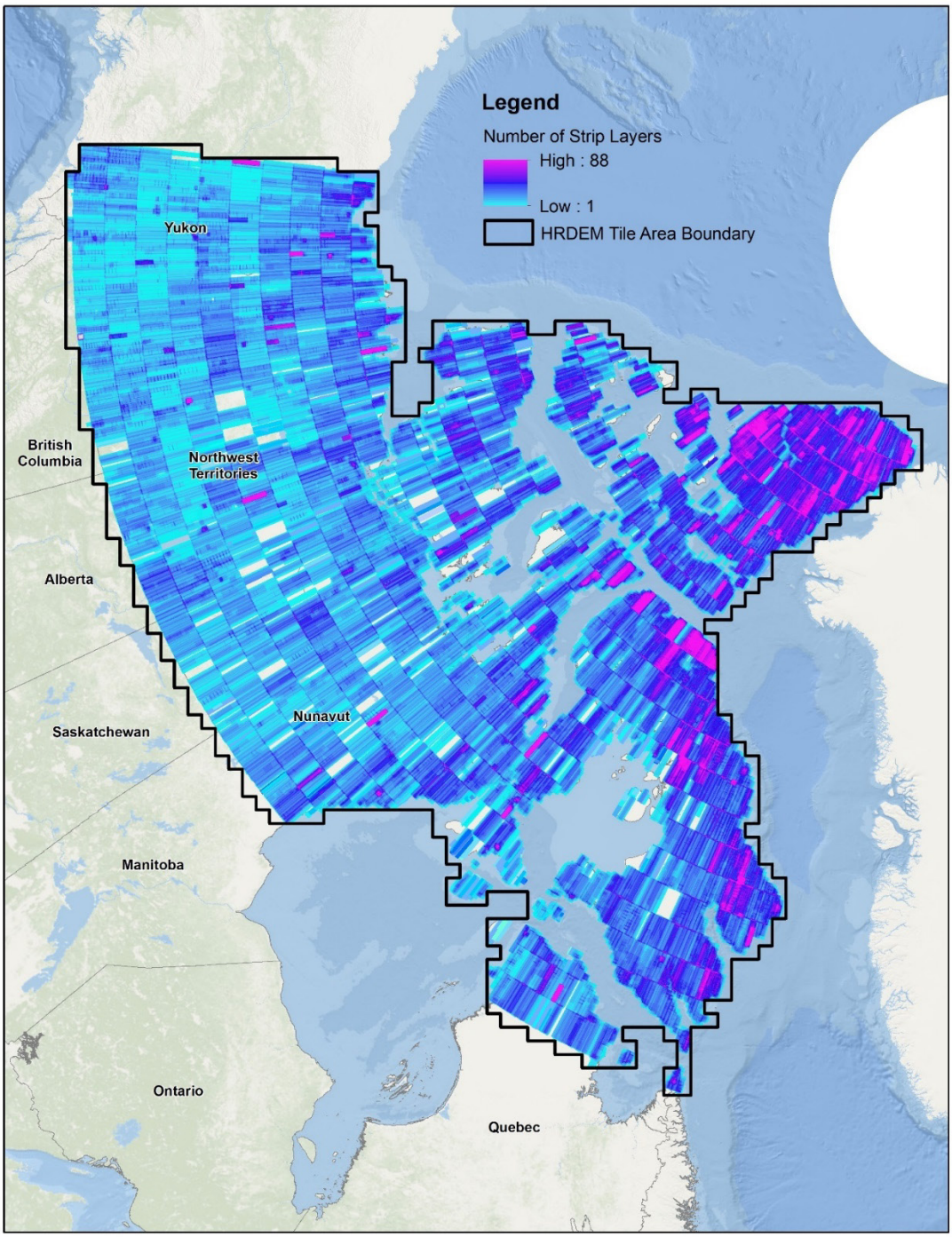

Figure 22. Density of strip data from the ArcticDEM v3 release 7 strip over HRDEM data anomalies

Title	ArcticDEM
Producer	Polar Geospatial Center–University of Minnesota
Description	A satellite based photogrammetric DSM over the Arctic
Product Type	DSM
Coverage Area	Arctic Region
Resolution	2 m
Accuracy	For version 3 release 7, for which the strips and mosaics were coregistered with ICESat points, vertical accuracy between 1.6 and 3 m (LE90) and horizontal accuracy of 5 m (CE90) for flat areas.
Coordinate Systems	WGS84 ellipsoidal height
Data Format	GeoTiff
Data Licensing	Open
Production Time	Version 3 release 7 was published in 2018. Estimated 2022 for the new version.
Cost	Free
Link	https://www.pgc.umn.edu/data/arcticdem/

Precision3D

Title	Precision 3D
Producer	Maxar Technologies
Description	Derived from satellite imagery elevation data. Maxar is building out the Earth using multiple satellite images to generate high resolution DSM data. Canada is currently not mapped but will be by 2024.
Product Type	DSM
Coverage Area	Global - Completed by 2024
Resolution	0.5 m
Accuracy	Vertical and horizontal accuracies <3 m (LE90)
Coordinate Systems	WGS84/EGM2008 geoid, Lat/Long or UTM
Data Format	GeoTiff 32 bit
Data Licensing	Commercial
Production Time	Ongoing - 2024
Cost	Yes
Link	https://www.maxar.com/products/precision3d-data-suite

AW3DEnhance

Title	AW3D Enhanced
Producer	NTTData Restec
Description	Data created from Maxar Optical Satellite Constellation. Minimum data order sizes is 25 km. Data is available off-the-shelf.
Product Type	DSM, DTM
Coverage Area	On Demand
Resolution	0.5 m, 1 m, 2 m

Accuracy	With GCP: vertical accuracy 1 m (RMSE)/horizontal accuracy 1.5 m (CE90) Without GCP: vertical accuracy 2 m (RMSE)/horizontal accuracy 3 m (CE90)
Coordinate Systems	WGS84/EGM2008 geoid, Lat/Long or UTM
Data Format	GeoTiff 32 bit signed floating point
Data Licensing	Commercial
Production Time	On Demand
Cost	Yes
Link	https://www.aw3d.jp/en/products/

NextMap One

Title	**NextMap One**
Producer	InterMap
Description	Global 3D terrain data hydro enforced. NEXTMap One, which is available as either DSM or DTM, is produced using Intermap's patented Intelligent Resolution Improvement System (IRIS™). IRIS generates a seamless global dataset using high-resolution satellite imagery along with multi-band radar, LiDAR and other datasets to produce NEXTMap One.
Product Type	DSM, DTM
Coverage Area	Global
Resolution	1 m
Accuracy	Vertical accuracy of 1 m (LE95)
Coordinate Systems	WGS84/EGM96 geoid.
Data Format	GeoTiff 32 bit
Data Licensing	Commercial
Production Time	Updated and on Demand (Intermap can generate 2 m DSM over the Canadian Arctic)
Cost	Yes
Link	https://store.intermap.com/MapShop.aspx?GeoLocation=World

Medium Resolution DEM (2–12 m)

WorldDEM Neo

Title	**WorldDEM Neo**
Producer	Airbus
Description	Satellite imagery data of continuing TanDEM-X mission primarily acquired from 2017 to 2021 and its derived auxiliary layers. WorldDEM™ Neo is based on information from the edited WorldDEM™ product (2010–2015, 0.4 arcseconds).
Product Type	DSM, DTM
Coverage Area	Global
Resolution	0.15" (~5 m)
Accuracy	Vertical accuracy <2 m for flat areas (LE90), horizontal accuracy <6 m (CE90)

Coordinate Systems	WGS84/EGM2008 geoid.
Data Format	GeoTiff 32 bit
Data Licensing	Commercial
Production Time	2017–2021
Cost	Yes
Link	https://www.intelligence-airbusds.com/imagery/reference-layers/worlddem/

NextMap Six

Title	**NextMap Six**
Producer	InterMap
Description	Global 3D terrain data hydro enforced. Intermap's patented Intelligent Resolution Improvement System (IRIS™) is used with satellite optical and SAR data.
Product Type	DSM, DTM
Coverage Area	Global
Resolution	6 m
Accuracy	Vertical accuracy <6 m (LE95)
Coordinate Systems	WGS84/EGM96 geoid.
Data Format	GeoTiff 32 bit
Data Licensing	Commercial
Production Time	Updated
Cost	Commercial
Link	https://store.intermap.com/MapShop.aspx?GeoLocation=World

AW3D Standard

Title	**AW3D Standard**
Producer	NTT DATA and RESTEC
Description	Data created from JAXA Advance Land Observing Satellite "DAICHI" (ALOS). Minimum data order size is 400 km2 (DSM) and 100 Km2 (DTM). Data is available off the shelf.
Product Type	DSM, DTM
Coverage Area	Global
Resolution	2.5 m, 5 m
Accuracy	Vertical accuracy 5 m (RMSE) and horizontal accuracy 7 m (CE90)
Coordinate Systems	WGS84/EGM2008 geoid, Lat/Long or UTM
Data Format	GeoTiff 16 bit signed integer or GeoTiff 32 bit signed floating point (available upon request)
Data Licensing	Commercial

Production Time	Started Feb 2014–ongoing
Cost	Yes
Link	https://www.aw3d.jp/en/products/

WorldDEM

Title	**WorldDEM**
Producer	Airbus
Description	The WorldDEM™ products are based on the "TanDEM-X Final DEM" produced by the DLR (RD-01). All post-processing procedures are performed by Airbus Defence and Space. The product usually contains radar-specific artifacts, voids and can include processing artifacts.
Product Type	DSM, DTM
Coverage Area	Global
Resolution	0.4 arcsec" (~12 m)
Accuracy	Vertical accuracy <4 m (LE90), horizontal accuracy <6 m (CE90)
Coordinate Systems	WGS84/EGM2008 geoid.
Data Format	GeoTiff 32 bit floating-point raster data
Data Licensing	Commercial
Production Time	2011–2015
Cost	Yes
Link	https://www.intelligence-airbusds.com/imagery/reference-layers/worlddem/

ICESat-2

Although not a raster DSM/DTM, ICESat-2 has been added to this list as elevation data with potential for improving the absolute accuracy of the HRDEM. Figure 23 shows an example of the density distribution of ICESat-2 swaths in 2019–2021 for June, July, and August over a part of Saskatchewan. A total of 168,064 elevation points were collected.

Figure 23 Example of ICESat-2 coverage between 2019 and 2021 and June, July, and August

ICESat-2 over land (green areas) is collected with sensor pointing away from repeat ground tracks to increase density of measurements over terrestrial surfaces (ICESat-2 Level3 product ATL08 (Neuenschwander, A., 2021). Figure 24 shows the coverage (in green) of ICESat-2 ALT08 data. The high Canadian Arctic regions will not be covered by this data.

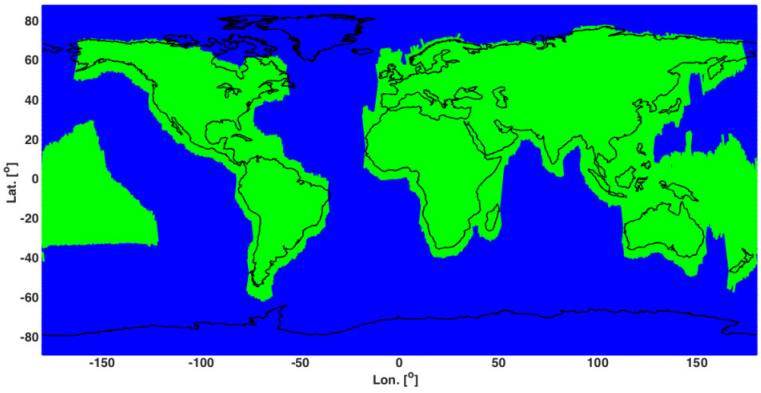

Figure 24 ICESat-2 off repeat ground track area in green for ATL08 Land - Vegetation Products

Title	ICESat-2
Producer	NASA
Description	ICESat-2 is a laser altimeter designed to accurately measure the height of snow and ice surfaces using green lasers with small footprints. ICESat-2 measures surface heights with six laser beams, grouped into three pairs separated by 3 km, with a 90 m separation between the beams in each pair. ICESat-2 flies a

	repeat orbit with 1387 ground tracks every 91 days. ICESat-2 data release version 5 ATL08 Land and vegetation height is current data available.
Product Type	Point Data
Coverage Area	Global - Does not cover the high arctic region (ATL08)
Resolution	13 m (footprint size)
Accuracy	Overall, the terrain heights from the ATL08 data product agreed with the airborne LiDAR with vertical errors less than 75 cm (mean = −0.07 m; MAE = 0.53 m, RMSE = 0.73 m; n observations = 909,467). ATL08 terrain heights had positive bias (33 cm) when permanent snow cover was present compared to the airborne LiDAR (Neuenschwander et al., 2020).
Coordinate Systems	Horizontal: WGS 1984 Vertical: WGS84 ellipsoidal height
Data Format	HDF5
Data Licensing	Open
Production Time	2018–ongoing (original mission was 3 years was achieved Jan 27, 2022)
Cost	Free
Link	https://nsidc.org/data/icesat-2

Low Resolution DEM (>12 m)

Aster Global DEM

Title	**Aster Global Digital Elevation Data**
Producer	NASA, METI/Japan Space Systems
Description	The first version of the ASTER GDEM, released in June 2009, was generated using stereo-pair images collected by the ASTER instrument onboard Terra. The improved GDEM V3 adds additional stereo-pairs, improving coverage and reducing the occurrence of artifacts. The refined production algorithm provides improved spatial resolution, increased horizontal and vertical accuracy. The ASTER GDEM V3 maintains the GeoTiff format and the same gridding and tile structure as V1 and V2.
Product Type	DSM
Coverage Area	ASTER GDEM coverage spans from 83 degrees north latitude to 83 degrees south, encompassing 99 percent of Earth's landmass.
Resolution	30-meter postings and 1 x 1-degree tiles.
Accuracy	The ASTER Global Digital Elevation Model Version 3 (GDEM v3) was evaluated over the conterminous United States in a manner similar to the validation conducted for the original GDEM Version 1 (v1) in 2009 and GDEM Version 2 (v2) in 2011. The absolute vertical accuracy of GDEM v3 was calculated by comparison with more than 23,000 independent reference geodetic ground control points from the U.S. National Geodetic Survey. The root mean square error (RMSE) measured for GDEM v3 is 8.52 meters (Gesch et al., 2016).
Coordinate Systems	WGS84/EGM96 geoid.

Data Format	GeoTiff 16 bit signed
Data Licensing	Open
Production Time	2019
Cost	Free
Link	https://search.earthdata.nasa.gov/search/

AW3D30

Title	**AW3D30 - ALOS World 3D-30 m**
Producer	JAXA EORC
Description	The data is built on ALOS World 3D (AW3D) cover global area acquired by PRISM panchromatic optical sensor on DAICHI (ALOS) as a 3D map of approximately 5m DSM. Data was used to create AW3D30. Version 2.2 from April 2019 focus in northern region 60 degree north. The current version is 3.2 (Jan 2022).
Product Type	DSM
Coverage Area	World
Resolution	30 m
Accuracy	In areas with low relief, the vertical accuracy was found to be 2.69 m (RMSE), while in areas with high relief the respective error rises up to 14 m (Nikolakopoulos, 2020).
Coordinate Systems	WGS84/EGM96 geoid.
Data Format	GeoTiff
Data Licensing	Notification to JAXA, credit for using the data, data ownership is JAXA, can be used for research and commercial services https://earth.jaxa.jp/en/data/policy/
Production Time	Survey date 2006–2011
Cost	Free
Link	https://www.eorc.jaxa.jp/ALOS/en/dataset/aw3d30/aw3d30_e.htm

PlanetDEM30

Title	**PlanetDEM30**
Producer	Planet Observer
Description	Produce from SRTM 30m and other source data (SRTM 1 Arc-Second, ASTER GDEM v2, NSIDC, AGDC, CDED, cartographic sources) and ALOS World3D 30m. 35% of earth tiles have been corrected.
Product Type	DSM
Coverage Area	Global
Resolution	30 m
Accuracy	Vertical and horizontal accuracies of 7 m (unknown level of confidence)
Coordinate Systems	WGS84/EGM96 geoid.
Data Format	GeoTiff

Data Licensing	Commercial
Production Time	Ongoing
Cost	Yes
Link	https://planetobserver.com/global-elevation-data/

Copernicus DEM

Title	**Copernicus DEM**
Producer	Germany, DLR and Airbus
Description	The Copernicus DEM is a DSM which represents the surface of the Earth including buildings, infrastructure and vegetation. This DEM is derived from an edited DSM version of WorldDEM, i.e. flattening of water bodies and consistent flow of rivers has been included. Editing of shore- and coastlines, special features such as airports and implausible terrain structures have also been applied.
Product Type	DSM
Coverage Area	Global
Resolution	30 m postings and 1 x 1-degree tiles.
Accuracy	Vertical accuracy <4 m (LE90) and horizontal accuracy <6 m (CE90)
Coordinate Systems	WGS84/EGM2008 geoid.
Data Format	GeoTiff; DTED
Data Licensing	Open–Non-commercial license
Production Time	Released in 2021
Cost	Free
Link	https://spacedata.copernicus.eu/web/cscda/datasets https://spacedata.copernicus.eu/documents/20126/0/GEO1988-CopernicusDEM-SPE-002_ProductHandbook_I1.00.pdf

FABDEM

Title	**Forest And Buildings removed Copernicus DEM (FABDEM)**
Producer	University of Bristol
Description	A new global DTM at 30 m grid spacing, with artifacts from forests and buildings removed (FABDEM) from the Copernicus Digital Elevation Model. Random forest machine learning models have been used to estimate anomalies in the terrain due to human settlements and forests.
Product Type	DTM
Coverage Area	Global
Resolution	30-meter postings and 1 x 1-degree tiles.
Accuracy	Over bare-earth regions, the accuracy of FABDEM will be identical to Copernicus DEM. The method to create the FABDEM reduces the mean absolute vertical error in built-up areas from 1.61 to 1.12 m, and in forests from 5.15 to 2.88 m
Coordinate Systems	WGS84/EGM2008 geoid.

Data Format	GeoTiff
Data Licensing	Open–Non-commercial license
Production Time	December 17, 2021
Cost	Free
Link	https://data.bris.ac.uk/data/dataset/25wfy0f9ukoge2gs7a5mqpq2j7

TERRITORIAL DEM DATA

Northwest Territories

The available elevation data in Northwest Territories (NWT) consist of primarily two datasets. The first is the airborne LiDAR collected between 2004 and 2021 shown in Figure 25. The collection locations are focused on corridors and site-specific collections such as communities or economic development sites.

NRCan is actively working with NWT to integrate LiDAR data acquired in recent years into national elevation products such as the HRDEM and the HRDEM Mosaic.

Figure 25. LiDAR captures from 2004 to 2021

The second dataset is 10 m DEM data shown in Figure 26 by larger white gridded tiles. The elevation data was acquired by NWT from Intermap. In addition, stereo imagery associated with small tiles were acquired by the Department of Lands–Commissioner of Lands. Typically, the mapping data request is to fly photogrammetric air photo and produce stereo data capture of planimetric features, including a DTM. Nominal 1:1,200 map scale requirements. Each community is updated every 3–4 years. An online web map application visualizes the data. https://www.lands.gov.nt.ca/en/services/explore-atlas-mapping

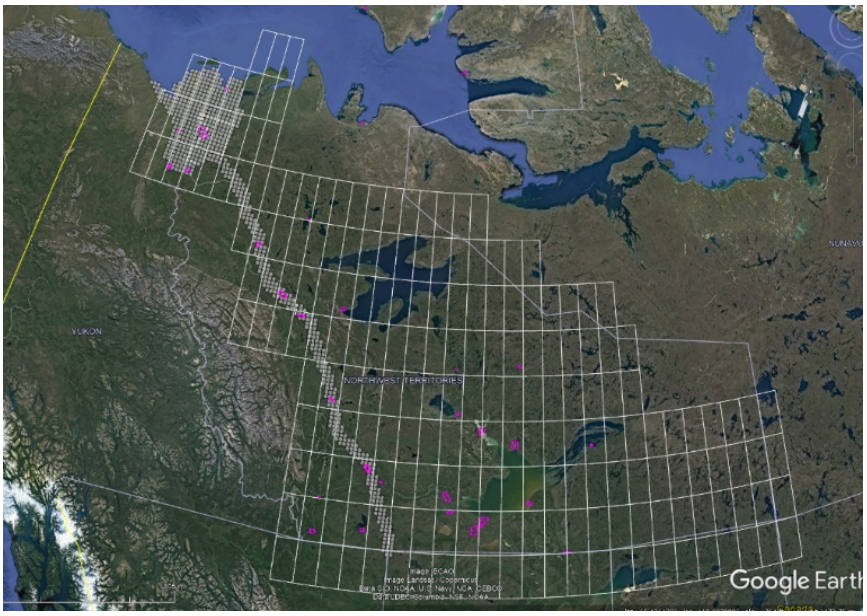

Figure 26. Intermap 10 m elevation data, community data and stereo imagery

Yukon

The primary source of elevation data in Yukon is airborne LiDAR data. The locations are shown in Figure 27 in red and yellow areas. Acquisition of LiDAR data has focused on the road corridors, communities, and utilities. No wide area elevation data collection has been conducted.

NRCan is actively working with the Yukon to integrate LiDAR data acquired in recent years into national elevation products such as the HRDEM and the HRDEM Mosaic.

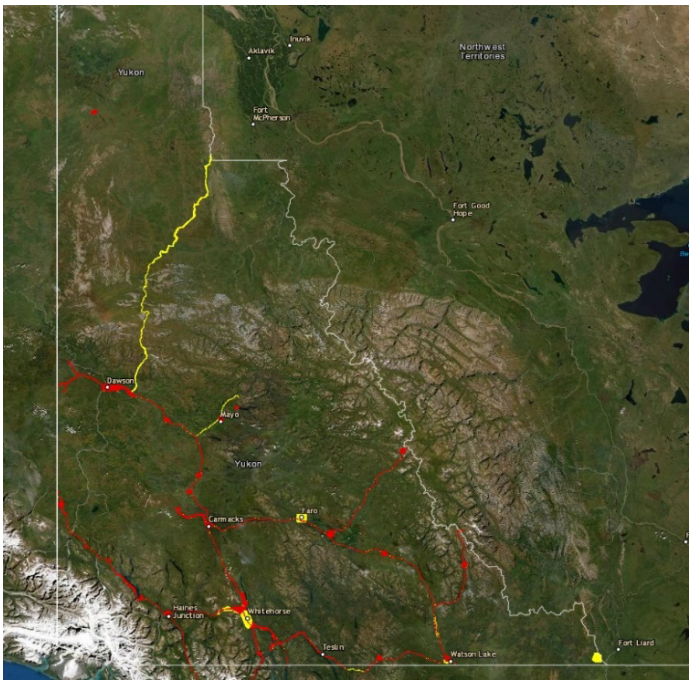

Figure 27. LiDAR collection in the Yukon

Nunavut

The location of available elevation data was not made available by the Nunavut Government, as no broad area mapping data has been conducted. Mapping has focused on community sites and selected corridor.

AVAILABLE ELEVATION DATA MAP

Two compilation maps of high to medium resolution elevation data were created to show available data and data on demand. Data search focused on spatial resolution ≤ 12 m. Majority of available (top map) and on demand (bottom map) cover the HRDEM area as shown in Figure 28.

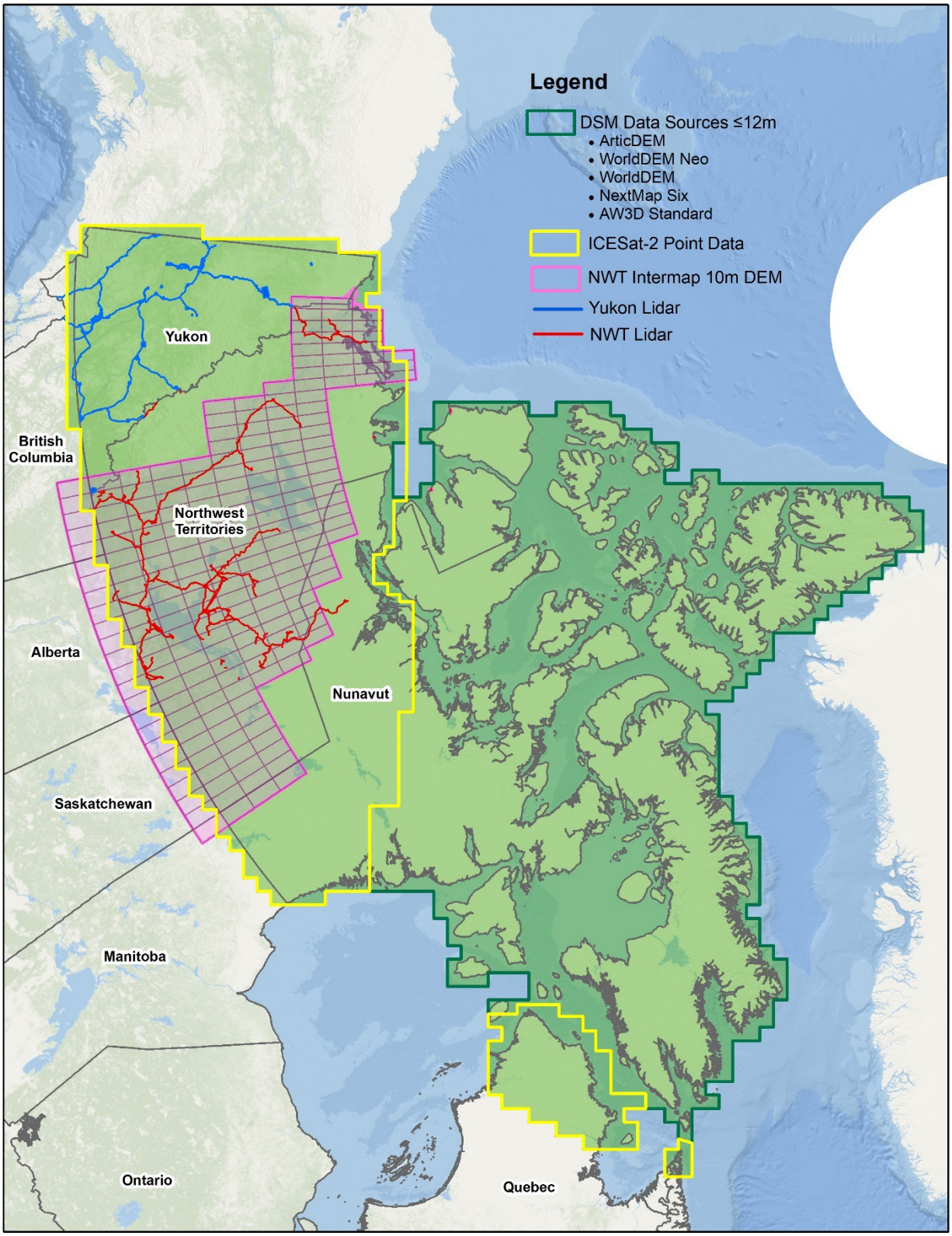
Legend
DSM Data Sources ≤12m
• ArticDEM
• WorldDEM Neo
• WorldDEM
• NextMap Six
• AW3D Standard
ICESat-2 Point Data
NWT Intermap 10m DEM
Yukon Lidar
NWT Lidar
Yukon
British Columbia
Northwest Territories
Alberta
Nunavut
Saskatchewan
Manitoba
Ontario
Quebec

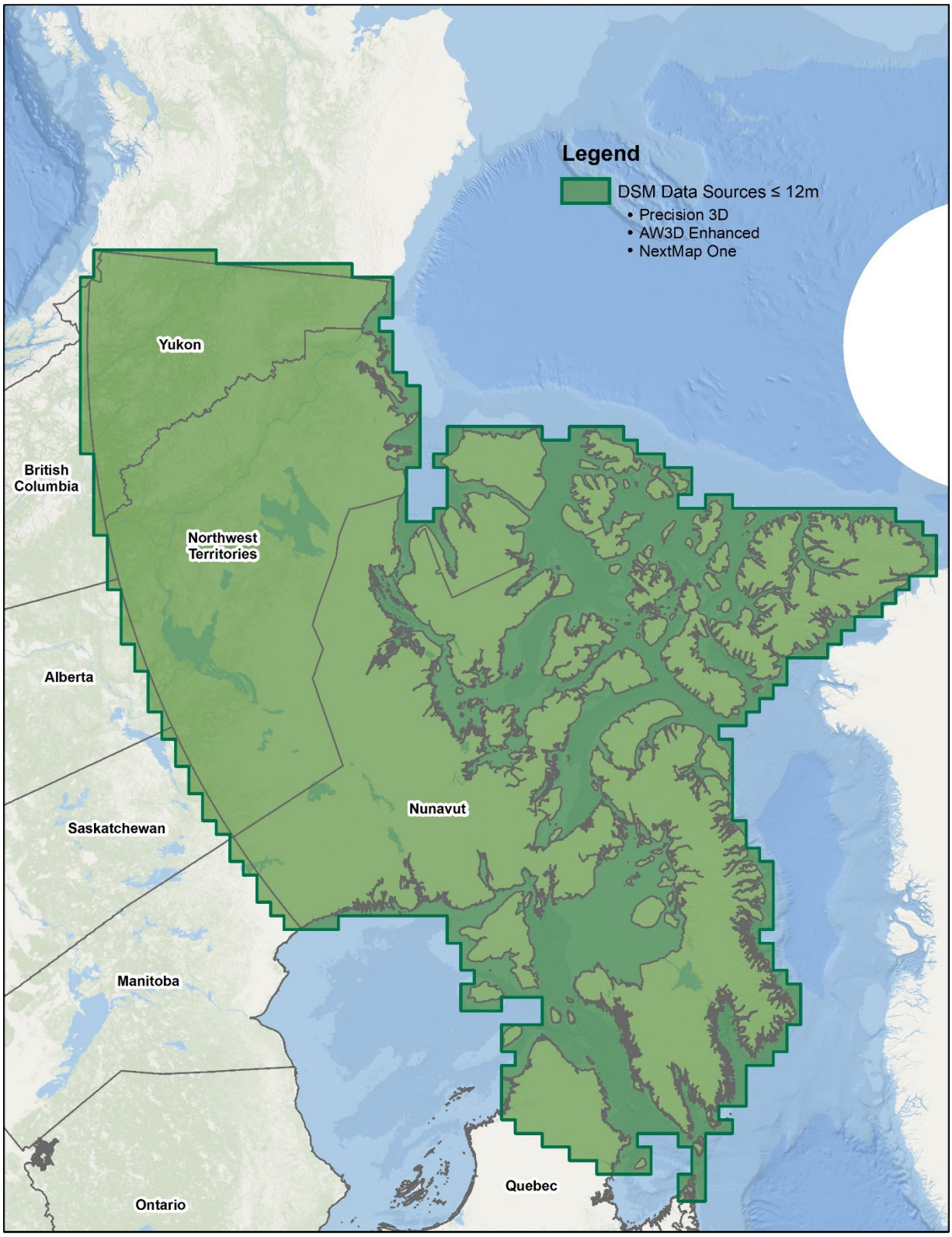

Figure 28 Available open source and commercial DSM data in HRDEM area. Top map represents available data and bottom map on demand DEM production.

NEW DEM DATA COLLECTION

Technologies available for large and remote area collection consist of airborne photon LiDAR, airborne InSAR, optical satellite imagery and SAR satellite imagery. A description of these technologies is provided below.

Airborne LiDAR Data

The vast area of Arctic region, challenging environment and limited airport facilities restricts the type of airborne LiDAR system suitable for collecting in HRDEM area. Corridors, community areas and infrastructure projects have used linear LiDAR system in Yukon and Northwest Territories. However, they have not been used for large area collections. Photon LiDAR systems that can fly higher, longer and faster than traditional linear LiDAR systems are considered more suitable for very large area collection. This section describes photon-based LiDAR systems.

Single Photon LiDAR

Single photon LiDAR (SPL) is a LiDAR technology that enables the acquisition of dense LiDAR point clouds using higher flight altitude and faster flight speed, enabling faster large area collections than traditional linear LiDAR.

SPL instruments typically operate in the green wavelength (532 nm) as opposed to near infrared (e.g. 1064 nm) used by conventional linear LiDAR instruments. This is because efficient single photon near-infrared detectors are not yet widely available. The Leica SPL100 system uses a 532 nm laser that is split into a 10 x 10 array of laser "beamlets" with the return energy received by a 10 x 10 array of single photon sensitive detector elements. This architecture enables the SPL100 to collect up to 6 million points per second with a 60 kHz pulse repetition frequency (PRF). Combined with moderate altitude collection campaigns (usually between 3,500 and 6,000 m), the SPL100 can collect at a 60-degree Field-of-View and can operate during the day and night. While the green wavelength is beneficial for bathymetry and ice-sheet mapping, it is not as optimal for vegetation and non-vegetation separation. The 532 nm wavelength leaf reflectance is much lower in the visible–green spectrum than in the near-infrared. Nonetheless, SPL collects multiple returns LiDAR data and very dense point cloud providing detail canopy and ground mapping, providing the capacity of deriving both DTM and DSM. Examples of canopy mapping is shown in Figure 29. When flown in leaf-on conditions, White et al. (2021) have shown that canopy penetration and therefore ground depiction can be an issue for SPL as compared to linear LiDAR systems. However, the vertical accuracy of this technology in both vegetated and non-vegetated environments is more than sufficient for the needs of the HRDEM in the North.

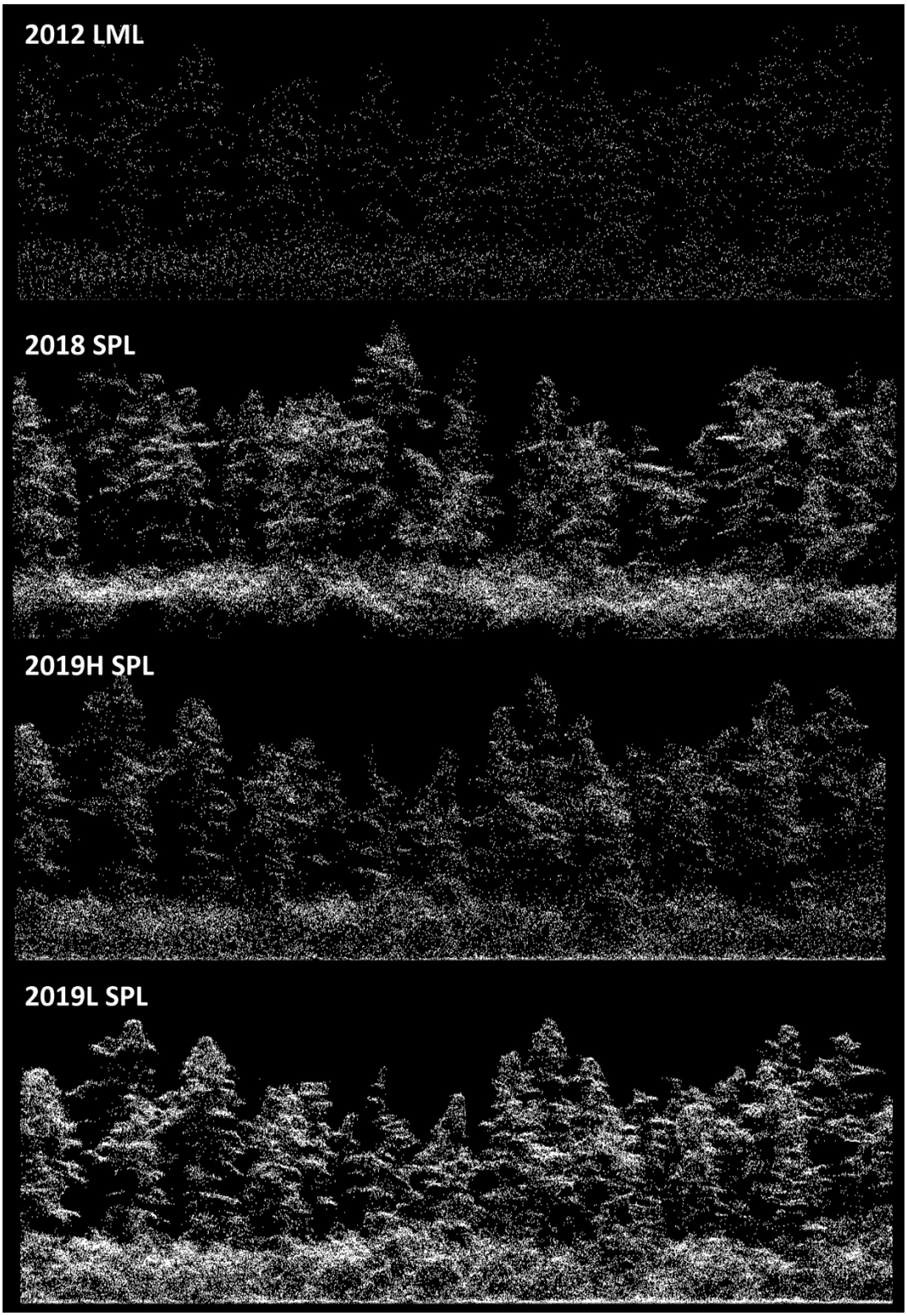

Figure 29. SPL100 Canopy mapping compared to linear LiDAR mapping (White et al., 2021). The same area is shown with linear LiDAR captured in 2012 in leaf-on conditions (2012 LML), single photon lidar with leaf-on conditions (2018 SPL), single photon lidar with leaf-off conditions collected at high altitude (2019H SPL) and single photon lidar with leaf-off conditions collected at low altitude (2019L SPL)

Hexagon operates seven SPL systems and has collected in Arctic regions in Europe. In addition, Hexagon has been extensively mapping forested areas in Northern Ontario. The project has spanned over a few years with a data collection area of about 250,000 km^2 as of summer 2022.

Depending on availability of sensors and aircraft and the size of the AOI, SPL data could be collected in the Arctic, as long as base operation can land and refuel the aircraft on paved runways. Hexagon has indicated that it is quite feasible to collect data without (or with limited) ground control. The most common way to do this is by generating trajectory data using "precise ephemeris" (precise orbit) data to provide GNSS position corrections. This data is generally available with increasing accuracy, depending on the wait time for the orbit data to be published. Generally, the orbit data released a few days after flight are of adequate accuracy (i.e., having only minimal, if any, effect on the accuracy of the resulting point clouds). This technique has been used with linear-mode LiDAR for years. Further to this, a subscription service (e.g., NovAtel TerraStar) can provide precise GNSS corrections in near-real time (i.e., available upon landing). The HxMap processing suite takes care of flight-line-to-flight-line adjustments.

Geiger Mode LiDAR

Another efficient technology for large area collection is the Geiger Mode LiDAR (GML) technology. The advantage of GML as a photon sensitive sensor is that it permits operating at much higher altitude for large area collections (usually between 4,000 and 8,000 m). GML is an array collection that observes ground targets in many directions and many times and has extremely sensitive measuring capabilities that can provide very dense high-resolution data, even up to 400 points per meter (ppm). Typical large collection point cloud density is about 30 pulses/m2. GML was originally developed for imaging through the canopy, thereby both DTM and DSM can be derived from GML. Figure 30 shows fallen trees detected on the forest floor under the canopy. When flown at very high altitude (~8 km) and in leaf-on conditions, Stoker et al. (2016) have shown that 3DEP standard lidar quality level 2 over vegetated areas (i.e. 30 cm, 95^{th} percentile) was difficult to obtain. In a recent study by Purdue University examining multi-platform LiDAR technology for Forest Resource Inventory (Lin et al., 2022), GML was flown at a much lower altitude (3 700 m) and in leaf-on conditions and was able to effectively characterize the terrain under the canopy. GML was also able to deliver forest attributes including individual tree counts, tree locations, and tree heights with accuracy comparable to those from the UAV LiDAR. The vertical accuracy achieved by this technology in both vegetated and non-vegetated environments is more than sufficient for the needs of the HRDEM in the North.

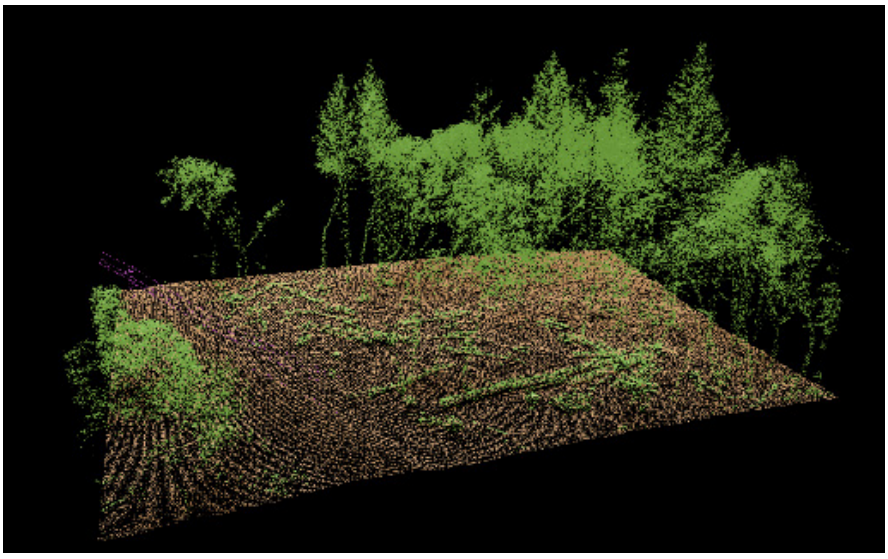

Figure 30. Geiger Mode-derived point cloud of a forest

In terms of sensor specification, GML is based on a Geiger Mode Avalanche PhotoDiode (GmAPD) sensor that precisely measures the Time of Flight (TOF) using Digital Timing Circuit. GmAPD is an array of sensors with 4096 individual detectors that, through a circular scanner known as Palmer Scanner, observes the ground in a 30-degree cone. GML is an active sensor where a laser is used to illuminate a scene. Based on prior knowledge of approximate distance to the target from sensors, a bias on the array is set known as arming which acts as a delay process. GmAPD is then charged up to desired overbias voltage. The array then operates in Geiger-Mode and a range gate is opened. Photons incident on a detector are converted to photoelectrons which may cause an avalanche effect, and a TOF count is triggered. Once the gate is closed, the overbias is removed, TOF values are read out and the array cycles for another observation. Figure 31 shows a diagram of the Geiger process.

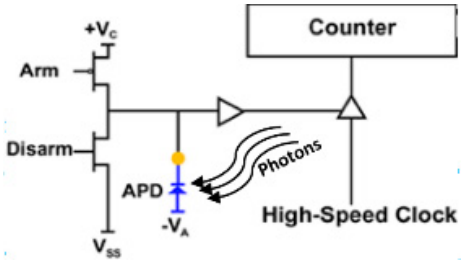

Figure 31. Geiger Mode Avalanche PhotoDiode Sensor

GML is best collected at night with low background light. The sensor collects first or only returns (i.e. no multiple returns). The current in-production systems can capture at a rate of 205 MHz or 205 million points per second from 50 KHz laser pulses. GML collects frames of overlapping LiDAR points and uses a block adjustment process to align collection areas. Collection of Ground Control Points is standard practice to increase horizontal and vertical accuracies on the order of centimeters, although they are optional. The rapid rate along with a significantly reduced pulse width of 550 picoseconds allows for small target detection and understory mapping.

GML sensors were originally developed for the US military. After declassification, L3Harris sold the technology to VeriDaaS, a Denver-based company in 2020. VeriDaaS has been operating three GML

sensors commercially. Acquisition with GML is using Metroline 23s and a Twin Commander which provide high altitude and fast collection. VeriDaaS has multiple sensors for large operational collection that can be used simultaneously.

1.1.1 Airborne SAR Data

SAR data is another alternative source for high-resolution DEM generation. In comparison with optical stereo images, high-resolution SAR datasets are favourable to produce DEMs with high accuracy and resolution for multiple types of regions as it is unaffected by illumination conditions (day and night) and weather conditions (Mercer, 2007).

DEM generation techniques based on SAR data can be divided into two categories: radargrammetry and interferometry (InSAR). Similar to optical stereo images, SAR radargrammetry relies on matching correspondences in the magnitude images of SAR data, which requires the acquisitions of two SAR images with sufficiently large difference in incidence angle (Meric et al., 2009). Compared to InSAR, SAR radargrammetry is less affected by atmospheric influence because SAR radargrammetry uses the magnitude value while InSAR uses the phase difference. Since magnitude is less affected than phase by atmospheric heterogeneity, the atmospheric disturbance is not much of a concern for SAR radargrammetry (Massonnet and Souyris, 2008). Nevertheless, SAR radargrammetry requires stereoscopic pairs of SAR images acquired from considerably different incidence angles. While very limited number of spaceborne SAR systems (i.e., COSMO-SkyMed, RADARSAT-2, TerraSAR-X) have the capability to acquire image data at different off-nadir incidence angles, airborne SAR systems are usually equipped with high-resolution and multiple off-nadir incidence angle capability, such as high-resolution DEM generation using the circular SAR (CSAR) data acquired by the SETHI system from ONERA (Baqué et al., 2017).

In general, higher accuracy of DEMs can be generated using the InSAR technique (Yu et al., 2010). As opposed to SAR radargrammetry, InSAR exploits the phase difference between two SAR images taken from slightly different sensor positions and extracts information about the Earth's surface. The phase is primarily determined by the distance between the satellite antenna and the ground targets. By combining the phase of two images after co-registration, an interferogram can be generated whereby the information is highly correlated to topography (Abdelfattah, R., & Nicolas, J. M. 2002). Although InSAR can generate high-resolution DEMs at meter-level accuracy, its success is highly subject to decorrelation, atmospheric disturbance, as well as the conditions on incidence angle and Doppler similarity are stringent (Meric et al., 2009). As opposed to SAR radargrammetry, InSAR DEM generation is based on the pixel-by-pixel differential phase and therefore is restricted to very similar incidence angles and is very sensitive to sensor movement (Toutin, T. & Gray, L. 2000).

Airborne SAR sensors, such as the F-SAR system from DLR, the PAMIR system from FGAN/FHR, the SETHI and RAMSES systems from ONERA offer high-resolution interferometric modes in X & C bands (Magnard et al., 2014), which are most widely used for high-resolution DEM generation. Besides that, some commercial companies also provide high-resolution InSAR data collection in X and/or C-band, for instance Fugro's GeoSAR, Intermap's STAR), Amigo Optima's MiniSAR and MetaSensing's MetaSAR.

One of the most recent airborne InSAR applications in the Arctic area is the 3DEP elevation mapping of Alaska, which was completed in September 2021. Specifically, 23% of Alaska, including the most rugged and densely forested areas, were mapped using the Fugro's P-band and X-band GeoSAR sensor, while the remaining easier 77% of Alaska were mapped using three Intermap's X-band STAR sensors. Fugro's perceived advantage was that the GeoSAR included both X-band and P-band (combined with GeoSAR's

LiDAR profiler) and thus could produce both DSM and DTM by penetrating the forest. However, Fugro did not have a mature production line for doing this. Intermap's advantage was that it had produced NEXTMap Europe, NEXTMap Britain, and NEXTMap USA over 49 states. It had a mature production line for delivering standard products that exceeded USGS specifications for mid-accuracy DEMs. Intermap's ortho-rectified radar images had 0.625 m resolution, whereas Fugro's ortho-rectified radar images had 2.5 m resolution. Mapping the easier terrain, Intermap routinely exceeded accuracy specifications whereas Fugro struggled to satisfy accuracy requirements, partly because the P-band didn't just penetrate vegetation, but sometimes also penetrated the ground, depending on soil wetness. Finally, the elevation product consisted of bare-earth DEM (DTM) and DSM and was compliant with USGS' QL5 level, equal to 5 m resolution and vertical accuracy <3 m (LE90) on low slope areas (0–10 degrees). More details on this project, including the total cost of this Alaska-wide project, is presented in Maune (2020).

As another example, Moller et al. (2011) reported a novel single pass InSAR technology under the GLISTIN-A NASA airborne mission, which can efficiently generate high-resolution DEMs over large spatial areas with a vertical accuracy ranging from 0.3 to 3 m and at a spatial resolution of 3 m. Moreover, Schumann et al. (2016) contributed to further improvement and achieved high-resolution DEMs with a vertical error of around 0.3 m at an average spatial resolution of 3 m. Instead of traditional X-band, Ka band was used in these two studies to yield higher spatial resolution DEMs. Further, Faherty et al. (2020) applied this technology for DTM generation with a vertical accuracy of 0.53 m (RMSE).

Besides the above examples, airborne InSAR data have been commonly applied for large-scale DEM generation, mainly aiming to overcome the limitation of airborne LiDAR data (clouds and daylight). Although LiDAR-derived DEMs provide high spatial resolution and acute vertical accuracy, the acquisition operations can be very costly for large scale and remote areas, and very difficult under cloudy and rainy conditions. Thus, airborne InSAR data have attractive growing attention since it allows to capture larger and remote areas more easily and under bad weather conditions. The compromise is a lost on spatial resolution and vertical accuracy as compared to LiDAR.

1.1.2 Optical Satellite Data

Besides LiDAR and SAR data, the generation of high-resolution DEMs can also be achieved from optical stereo images. It's worth noting that from this technology, only DSM can be generated, although post-processing can be applied to remove elements at the surface to generate an estimated DTM. As explained before, the current HRDEM in the North is based on DEMs derived from high-resolution optical satellite stereo images (i.e. ArcticDEM). In this section, we focus on the availability, characteristics, advantages and disadvantages of high-resolution optical satellite images for high-resolution DEM generation.

In recent years, there is an increasing demand for using very high-resolution optical satellite images for large-scale topographic mapping and digital terrain product generation. Compared to other optical satellites, very high-resolution satellite images have several advantages in DEM generation. First, very high-resolution images make it feasible to yield high-resolution DEMs with significantly improved horizontal and vertical accuracies. Second, extremely long camera focal length effectively captures surface relief information from satellite orbit (Deilami and Hashim, 2011). Moreover, their agile pointing ability enables the generation of same-date along-track stereo images, reducing radiometric image variations and so improving the success rate during the image matching process (Toutin, 2004). Further, the opportunity of revisit frequency of 1 to 5 days minimizes temporal disturbances with the image scene. Last but most importantly, the adaptable stereo imaging capability of very high-resolution optical satellites allows generating strong stereo geometry with most ever available overlapped area and base-to-height ratio (B/H)>0.5. It is commonly believed that satellite imaging geometry, in particular B/H ratio

or convergence angle, plays a significant role in the improvement of DEM vertical accuracy (Aguliar et al., 2013). On the other hand, smaller B/H ratios may be preferred in city areas to increase similarity between the two stereo images and thus improving the matching stage (Eckert and Hollands, 2010). Beside B/H ratios, quantity and quality of GCPs as well as the relief of the area of interest can significantly affect the horizontal and vertical accuracies of DEM generation (Hu et al., 2016).

There are several limitations that reduce the application of optical satellite images for high-resolution DEM generation that include, insufficient GCPs, imprecise ephemeris data, steep terrain, and cloud conditions (Deilami and Hashim, 2011). However, DEM generation in the Arctic is a viable solution for selected land cover areas as demonstrated in ArcticDEM project which was based on the WorldView and GeoEye constellations. Sections 9 and 10 from the current report presents a thorough investigation of the issues encountered with this technology in the Canadian arctic context.

In the common workflow of DEM generation using very high-resolution stereo images, mathematical models are first used to georeference the stereo images. Usually, the RPC model is first used for image georeferencing as a generic sensor model, then further refined by the GCPs. The georeferencing is thereafter followed by image matching, where common pixels in the overlapped area of stereo images are identified and measured for DEM generation. For example, the Ontario DEM was generated by implementing the pixel-autocorrelation method for stereo aerial image matching (Ontario Report, 2022).

In this section, several very high-resolution satellite sensors are reviewed and compared for DEM generation, in terms of spatial resolution, revisit interval, data coverage, single-pass stereo, viewing angle, horizontal and vertical accuracies (Table 6). Note that CE90 is the circular error at 90% confidence interval. This means that there is a 90% probability that the horizontal error is better than the stated CE90 value. LE90 is the 90th confidence interval linear error, meaning that there is 90% probability that the vertical error falls within the stated LE90 value.

Specifically, for Maxar image products (e.g., GeoEye-1, WorldView-1, 2, 3), basic stereo pair imagery products are suitable to create DEMs for three-dimensional feature extraction. The satellite data are georeferenced using refined satellite attitude and ephemeris information. A horizontal geolocational accuracy of 5 m (CE90), excluding terrain and off-nadir effects, can be achieved at less than 30° off-nadir when *Image Support Data* (i.e. RPCs) is used. Using basic stereo imagery for generating DEM, image products are radiometrically, and sensor-corrected and when *Image Support Data* is provided, a vertical accuracy of 5 m (LE90) at less than 30° off-nadir can be expected (Digital Globe (n.d.)). Other assessments of the DEMs derived from the Maxar optical satellite imagery without refinement with GCPs have shown vertical accuracy between 1.6 and 2.8 m (RMSE) (Mulawa et al., 2018). As suggested by Wang et al. (2019a), the vertical accuracy of DEM generation using WorldView-2 stereo images can reach 0.25 m when appropriate GCPs are used to improve image geo-positioning. Another experiment reported by Saldaña et al. (2012) indicated that the horizontal and vertical accuracies of DSM generated from GeoEye-1 stereo images were better than 0.5 m. For the ArcticDEM datasets version 3 release 7, which were based on GeoEye and WorldView constellations imagery, both the strips and the mosaic DEMs were coregistered to ICESat. Candela et al. (2017) have shown a vertical accuracy around 1 m (RMSE) for the ArcticDEM strips over flat terrain, after coregistration to ICESat altimetric points. This accuracy can be slightly worse over more challenging terrain or areas with snow cover at the moment of acquisition. This range of vertical accuracy was confirmed on the mosaic DEMs through internal works by CCMEO (not published) over different flat Canadian arctic sites.

For Airbus image products (e.g., SPOT, Pleiades, Pleiades Neo), single-pass stereo images are available for high-resolution DEM generation. The spatial resolution, revisit interval, data coverage, viewing angle, and horizontal accuracy of Pleiades Neo stereo images are matchable to the Maxar image products (See Table 6). As reported by Zhou et al., (2015) the vertical accuracy of DEM extracted from Pleiades 1A and 1B stereo images can reach 0.3 m when GCPs are used. In another study conducted by Berthier et al. (2014), the potential of sub-meter Pleiades 1A and 1B stereo images was evaluated to derive DEMs of glaciers and their elevation changes. The vertical accuracy of the yielded DEMs was less than 1 m (RMSE) with GCPs used. Moreover, as mentioned in this paper (Berthier et al., 2014), the Pleiades images have a higher radiometric resolution (i.e., 12 bits) than the Maxar products (i.e., 11 bits) so can be less saturated for high-resolution DEM generation over very while areas, such as glaciers and snow areas.

For BlackSky image product (e.g., Global), single-pass stereo images are not available at the moment so not appropriate for high-resolution DEM generation.

Table 6 Optical satellite sensor parameters for high-resolution DEM generation (without independent GCP corrections applied, unless said otherwise). Values are derived from product specifications and from the following literature references: (DigitalGlobe, nd; Airbus, nd; Berthier et al., 2014; Mulawa et al., 2018; Nonin et al., 2013)

Satellite Company	Optical Satellite	Resolu-tion (Panchro) meters	Revi-sit	Coverage	Single-pass Stereo	Tri-Stereo	View Angle	Horizontal Accuracy (RMSE)	Horizontal Accuracy (CE90)	DEM Vertical Accuracy (RMSE)	DEM Vertical Accuracy (LE90)
Maxar	GeoEye-1	0.41	2.1 days	Anywhere	Y	N	15–30	1.9 m	3.0 m	1.6 m	2.8 m
	WorldView-1	0.5	1.7 days	Anywhere	Y	N	15–31	2.4 m	3.6 m	1.6 m	2.6 m
	WorldView-2	0.46	Daily	Anywhere	Y	N	15–32	3.1 m	5.1 m	2.8 m	4.4 m
	WorldView-3	0.31	Daily	Anywhere	Y	N	15–33	2.6 m	3.9 m	1.8 m	3.0 m
Airbus	Pleiades 1, 2	0.5	Daily	Anywhere	Y	Y	26.5	N/A	<6.5 m	<2–3 m	<3–5 m
	Pleiades Neo 3, 4, 5, 6	0.3	Daily	Anywhere	Y	Y	27	N/A	<5 m	N/A	N/A
	SPOT 6, 7	1.5	Daily	Anywhere	Y	N/A	26.5	N/A	<35 m, down to 1–2 m when corrected with GCPs (Nonin et al., 2013)	N/A	~3 m (with GCPs used, from Nonin et al., 2013)
BlackSky	Global	1	N/A	N/A	N	N/A	N/A	N/A	<20 m	N/A	N/A
Planet	RapidEye	3.125	N/A	N/A	N	N/A	N/A	N/A	N/A	N/A	N/A
	Dove	5	Daily	Anywhere	N	N/A	N/A	N/A	N/A	N/A	N/A
	SkySat	1	Sub-daily	Anywhere	Y	Y	27	<30 m	NA	N/A	N/A

1.1.3 SAR Satellite Data

The application of satellite SAR data share the same theory as airborne SAR data for high-resolution DEM generation. Since very limited number of spaceborne SAR systems (i.e., COSMO-SkyMed, RADARSAT-2, TerraSAR-X) provides multiple off-nadir incidence angle capability (Raggam et al., 2009), this section focuses on high-resolution DEM generation using SAR interferometry (InSAR) instead of SAR radargrammetry.

In recent years, a new generation of high-resolution SAR satellites became operational such as TerraSAR-X, TanDEM-X, COSMO-SkyMed, ICEYE, RADARSAT-2, and Radarsat Constellation Mission (RCM), which makes it possible to generate high-resolution DEMs (Watanabe et al., 2011). For example, Sefercik (2013) used TerraSAR-X high-resolution Spotlight images for 3 m DEM generation in complex geometry of urban

settlements and achieved vertical accuracy ranging between 7.09 and 8.11 m (RMSE). Moreover, Lombardi et al. (2016) took advantage of COSMO-SkyMed high-resolution Spotlight images to produce 3 m DEMs and achieved vertical accuracy of 3 m (LE90).

One of the most recent applications is WorldDEM Neo, which was conducted by Airbus during 2017–2021. Twin satellites of TerraSAR-X and TanDEM-X collected the satellite InSAR data for high-resolution DEM generation. As a result, WorldDEM Neo provides seamless pole-to-pole coverage and standardized global DEMs with no regional or national border divides. The WorldDEM Neo has been developed based on the WorldDEM product, which has a lower spatial resolution of 12 m and a lower vertical accuracy of 4 m. With the improved techniques, the elevation product of WorldDEM Neo has a 5 m spatial resolution and guarantees a vertical accuracy of <2 m LE90 (0–20 degrees of slope), <4 m LE90 (>20 degrees of slope), and a horizontal accuracy of <6 m CE90 (Airbus, 2021).

Besides the twin satellites of TerraSAR-X and TanDEM-X operated by Airbus, COSMO-SkyMed, ICEYE, RADARSAT-2, and RCM (Table 7) are alternative satellite InSAR data sources for high/medium resolution DEM generation. Nevertheless, orbit control and Doppler pointing of the current ICEYE satellite were found no good enough to support reliable InSAR technic. Moreover, the RCM satellite is not appropriate for InSAR-based DEM generation due to the fact that RCM satellites fly inside an orbit tube of 120 m (radius), which gives a maximum InSAR perpendicular baseline of 240 m. That configuration optimizes surface deformation and coherence change detection applications as design choice, but it is not good for DEM production (Charbonneau, personal communication, 2021). The RADARSAT-2 satellite is also not optimal because its revisit time is 24 days, which increases the chances of low coherence between two images when using the InSAR technique. Meanwhile, the RADARSAT-2 data can be used for DEM generation using SAR radargrammetry. However, the vertical accuracy is not acceptable for high-resolution DEMs. Specifically, the technique of SAR radargrammetry was utilized to generate DEMs in a challenging mountainous Canadian Arctic region using the RADARSAT-2 data (Clavet et al., 2011; Toutin et al., 2012) but the vertical accuracy was only around 20 m (LE68). Over low relief terrain surrounding Barnes Ice Cap on Baffin Island, Papasodoro et al. (2016) used a similar RADARSAT-2 radargrammetry approach and measured a vertical accuracy of 7 m (LE68) and a vertical bias of 4 m. These papers give an overview of the accuracy that can be expected for various types of terrain in the Canadian Arctic using SAR radargrammetry.

Table 7 RADAR satellite sensor parameters for InSAR DEM generation

Satellite Company	RADAR Satellite	Image spatial resolution, meters	Re-visit	Coverage	Band	DEM Horizontal Accuracy (CE90)	DEM Vertical Accuracy (LE90)
Airbus	TerraSAR-X	0.25 to 2 (Spotlight modes)	4–7 days	Global	X	<6 m	<2–4 m
	TanDEM-X	0.25 to 2 (Spotlight modes)	4–7 days	Global	X	<6 m	<2–4 m
ASI/MoD	COSMO-SkyMed	1 (Spotlight)	5 days	Global	X	N/A	3 m
ICEYE	ICEYE	1 (Spot)	Daily	Global	X	N/A	N/A
CSA/MDA	RADARSAT-2	1 x 3 (Spotlight)	24 days	Global	C	N/A	N/A
	RCM	1 x 3 (Spotlight)	4 days	0.95	C	N/A	N/A

Overall, both optical stereo images and InSAR data show advantages and disadvantages but have similar accuracy values that are of the same magnitude than the current HRDEM in the North. Regardless of the cost of data collection, DEM generation using optical stereo images usually achieve high horizontal and vertical accuracy in relatively flat areas, while InSAR data gains the advantage of data availability and performs better accuracy in mountainous areas (Hoja et al., 2007). Compared to the satellite InSAR data, airborne InSAR systems have the advantage of flexible flight, high spatial resolution, and high accuracy of interferometric acquisitions (Wang et al., 2021). The wavelength of InSAR data can vary based on the type of surveyed area. For example, P-band can be used for high-resolution DEM generation over forested areas instead of X or C bands because P band is better at the penetration into vegetation canopies, thus allowing generating DTM.

DEM PROCESSING METHODOLOGIES

This section provides an overview of different processing methodologies that can be used for correcting anomalies in the HRDEM data.

An overview of DEM processing methods to address correction to HRDEM is shown in Figure 32.

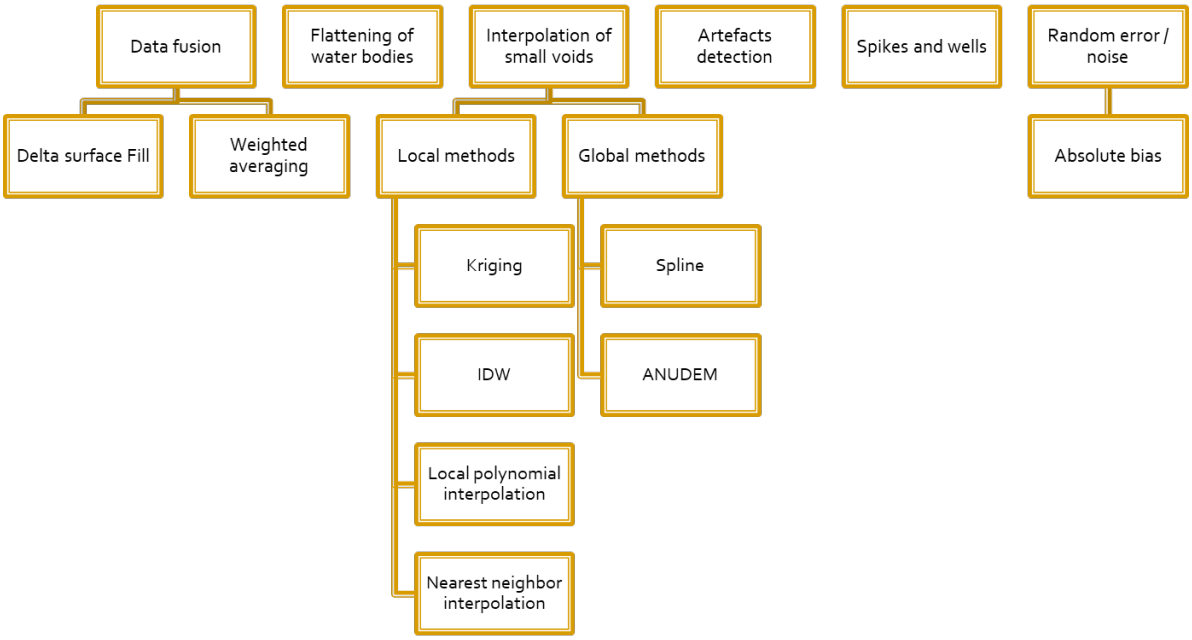

Figure 32. DEM Processing Methodologies

Analytical Methods

Depending on the type of anomalies, existing analytical DEM enhancement techniques can be categorized into the several categories described in this section.

Data Fusion Strategies for Large Voids

Airbus Defense and Space defined a large void as any void larger than 16 contiguous pixels (Collins et al., 2015). It is a reasonable reference and has been used throughout this section of the report. Interpolating a large void can cause undefined results and artifacts (Reuter et al., 2007), hence data fusion is necessary. In this case, a complementary DEM data source is integrated with the void-prone DEM. Data fusion can drastically improve the quality of a DEM, but it can pose difficulties. Namely, the two DEMs need to correspond perfectly. This can be a challenge to achieve as there are factors that can cause DEMs to deviate with respect to one another like DEM generation technology (LiDAR, RADAR, images, etc.) or horizontal accuracy. In this section we will present common data fusion algorithms in the context of DEMs. Specifically, focus is put on established techniques that have been used for processing common global DEMs and country-wide DEMs.

Delta Surface Fill (DSF)

DSF is one of the most established algorithms for DEM fusion. It was originally used for editing the SRTM DEM and then became state-of-the-art in this regard. The DSF algorithm has good performance for moderate-relief terrain and its accuracy decreases over mountains and rough surfaces.

DSF starts by resampling the ancillary DEM to match the original grid DEM in the projection, datum, and resolution using an interpolation technique. The bilinear interpolation was used in the original DSF. The difference between the 2 DEMs is computed (called a delta surface). This surface has voids that coincide with the original DEM. Then the centre area of a large void in the delta surface is assigned a constant value equal to the mean value of the overall difference using a 20–30 pixels distance. The remaining voids in the delta surface (small voids) and areas between the void edge and the centre are filled with interpolated values using an interpolation technique (inverse distance weighting was used in the original implementation). Finally, the interpolated Delta Surface is combined with the fill source DEM through addition and placed inside the void. Figure 33 illustrates the steps of the DSF method.

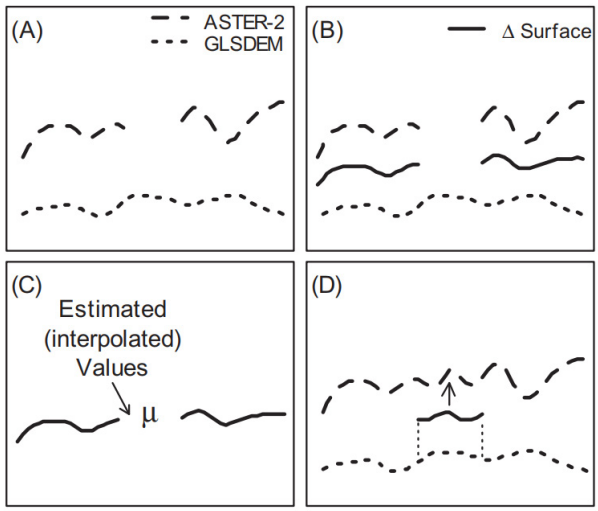

Figure 33. DSF method. In this example, GDEM2 and GLSDEM are the input data (A) They are subtracted to create the delta surface (B) The mean delta value is inserted in the centre of the voids in the delta surface and the surrounding pixel values are estimated through interpolation (C) The delta surface is combined with the original DEM (D) (Robinson et al., 2014)

DSF is relatively simple to implement. An open source implementation in python is available from (Sosa, 2018, 2019). The delta surface method has more accurate estimates than traditional void-filling approaches, like the fill and feather approach, because the latter cannot account for varying vertical biases within the void. Therefore, it was used for processing WorldDEM by Airbus (Collins et al., 2015). The original DSF algorithm can be improved upon using various techniques:

- Anchoring the reference DEM to the source one over specific-tie points selected by discarding unreliable pixels. All unreliable pixels are treated as if they were voids, including spikes. This enables the computation of non-rigid shifts between the two DEMs. These modifications were used for editing the TanDEM-X Global DEM (González et al., 2020).

- Adding a low pass filter to smooth the delta surface after the interpolation filter. This was used for editing the TanDEM-X Global DEM (González et al., 2020).

- Using a triangular irregular network that could better handle the varying altitude biases between different DEM datasets (Luedeling et al., 2007). This variation was used to fill the SRTM voids using digitized topographic maps in a mountainous area where the absolute elevations are not accurate, whereas the elevations of topographic features relative to the surrounding area are more likely to be good. The TIN was used to extract these relative elevations and combine them with the SRTM model.

- An interesting modification to the DSF making it capable of using an ancillary DEM with voids. This was used for processing the new version of GDEM3 (Abrams et al., 2020).

- Filling the delta surface voids via an iterative edge-growing interpolation scheme (Siemonsma, 2015). This was used for processing the SRTM V3 (Farr et al., 2007) and the NASADEM (Crippen et al., 2016).

- Changing the interpolation method of the delta surface. For example, 3 second SRTM Digital Elevation Model (DEM) of Australia used natural neighbour interpolation instead of inverse distance weighted interpolation. Also, the mean plane inside larger voids was not used ("The Commonwealth Scientific and Industrial Research Organisation," 1997) and the National Center for Ecological Analysis and Synthesis used regularized spline with tension interpolation to create the EarthEnv-DEM90 (Robinson et al., 2014), a global DEM providing some coverage in high latitudes.
-

Weighted Averaging

A simple weighting scheme can be used to fuse the overlapping portions of DEMs by taking the average of all available overlapping DEMs at each pixel. The reason is because a simple averaging can be inaccurate since large errors can skew the average. The solution then is to use weights.

The weights can be derived from image geometry (accuracy) or height error maps for DEMs generated from RADAR for example (Fuss, n.d.). For DEMs derived from satellite images, the weights can be derived from the mean standard deviation and the density of matched points in the DEM generation process. Weights can also be computed from some DEMs measures like slope, aspect or roughness, or land cover classes like buildings, streets, bare ground, water, etc. (Papasaika et al., 2009). The main weakness of weighted averaging is that it looks at each grid point independently, disregarding the resulting surface shape; and on the other hand, that the up-sampling of one of the input DEMs could potentially introduce further artifacts (Schindler et al., n.d.).

A similar procedure was used by the German aerospace centre (DLR) for improving the quality of the TerraSAR-X DEM based on height error maps (Huber et al., 2021). The above fusion techniques need to be followed by a feathering procedure at the edges so that the transition between the DEMs is seamless. Table 8 illustrates the data fusion procedures used for some of the global and country DEMs, the ancillary data used, and relevant information related to the data fusion method.

Table 8 Data fusion technique per global and country DEM

Data fusion technique	Country	DEM	Ancillary DEM used for void filling	Relevant information
Delta surface method (DSF)	Global	EarthEnv-DEM90 (Robinson et al., 2014)	- ASTER GDEM2 - CGIARCSI SRTM v4 - GLSDEM	
		WorldDEM (Collins et al., 2015)	- SRTM / ASTER GDEM	

		TanDEM-X Global DEM (González et al., 2020)	- Local LiDAR DEM - SRTM DEM - ALOS - NASADEM	Use tie points to anchor reference DEM to the source followed by a low-pass filter to smooth the delta surface
		GDEM V3 (Abrams et al., 2020)	- GDEM V2 - SRTM	
		NASADEM	- GDEM V2	
	Australia	3 second SRTM Digital Elevation Model	- GEODATA 9 second DEM	Use natural neighbour interpolation for the delta surface instead of inverse weighted distance
Weighted averaging	Global	TanDEM-X Global DEM (Huber et al., 2021)	- SRTM and/or ASTER GDEM	
	Global	MERIT DEM	- SRTM - ALOS	

These techniques generally assume the presence of a good quality ancillary DEM and global elevation models are only available at coarse resolutions. For example, ArcticDEM has a spatial resolution of 2 m; consequently, data fusion strategies should only consider similar DEMs. These data sources are offered through commercial third parties. At the same time, there are global DEMs with a coarse resolution like ASTER or SRTM.

For the HRDEM, 35% of void areas span less than 1 square kilometer. Consequently, 65% of total voids are large necessitating data fusion strategies. 125 of those have an area between 10 and 20 km^2 and 4 individual voids have an area bigger than 1000 km^2. These are mainly located in the Yukon and the Northwest Territories. In the north and northeast, voids are relatively small with a maximum area of 12 km^2. There are small voids scattered across the HRDEM coverage. For some of the large voids, the density of strips from the upcoming ArcticDEM release is high and thus we can expect the area of large voids to decrease after the new ArcticDEM release. For the remaining voids, using one of the data fusion algorithms, namely DSF or weighted averaging poses the challenge of having access to a good high quality auxiliary DEM, especially as all the high-resolution DEM are commercial solutions.

If a commercial solution is considered (NextMap One for example), the original DSF implementation with a bilinear interpolation is sufficient as the auxiliary DEM resolution is high. If a commercial solution is not possible, DSF based on the Global DEM combined with a good super-resolution technique to enhance its spatial resolution should be considered. Though machine learning techniques can be used to increase a DEM resolution, results obtained by Müller et al. 2020 show that cubic up sampling is enough in most scenarios.

Flattening of Water Bodies

Water bodies sometimes appear as noisy or invalid values. The goal is to achieve a constant height level of these areas. This process is called hydro-flattening. Specifically, water bodies such as streams, rivers, and long reservoirs need to show an elevation change along their length, whereas ponds, lakes, or other cartographically polygonal water surfaces need to show a static water surface. However, first classifying these areas into ocean water, lakes and rivers should be considered. The difficulty in processing water bodies lies in the mask used to select them. This mask should be based on data acquired

concurrently, or as close as possible to the DEM acquisition given the high variability of water surfaces in time. Furthermore, for ocean water, the coastline must be accurately detected with a coast detection algorithm.

It should be noted that the HRDEM in the North was already almost completely hydro-flattened (see Section 7 of the current report for more details)

To enumerate common algorithms used, a distinction must be made between inland and ocean waters:

- Inland water: This category includes lakes and rivers.
    - Lakes: lakes must be identified using an accurate and up-to-date water mask. Then, the pixels inside the mask will be assigned a constant height value based on the values of the lake perimeter. To avoid underestimating the height value by taking the lowest elevation along the perimeter, the 20^{th} percentile can instead be chosen (Huber et al., 2021). A similar procedure was used for processing WorldDEM (Collins et al., 2015). The ASTER Global Water Body Database (ASTWBD) was generated to correct elevation values of water body surfaces like oceans, rivers, and lakes (Abrams et al., 2020). It used proprietary software to extract water bodies from the ASTER images used to create the GDEM and then the elevation for each lake was calculated from the perimeter elevation data using the mosaic image that covers the entire area of the lake.
    - Rivers: rivers elevations are set in a similar manner to lakes, with the exception that rivers must flow downhill monotonically. To do this, supporting points along the course of the river centred in the middle of the stream must be identified, the elevation of these points is derived from the bank's height like the lakes and then a slight and continuous slope can be achieved along the river (Huber et al., 2021). In ASTER GDEM (Abrams et al., 2020), rivers presented a unique challenge, because their elevations gradually step down from upstream to downstream. Initially, visual inspection was required to separate rivers from the lakes. A stepwise elevation assignment, with a step of one meter, was carried out by manual or automated methods, depending on the situation.

- Ocean: to add elevation values to these areas, a simple georeferencing to the geoid height can be performed (González et al., 2020). Thus, the most important input for the ocean flattening is a map containing the geoid heights of the Earth with reference to an ellipsoid like WGS84 using EGM2008 Geoid Model. For the ASTER Global Water Body Database (ASTWBD), the effect of sea ice was manually removed to better delineate ocean shorelines in high-latitude areas. This process was enhanced by reference to Google Earth and GeoCover images (Abrams et al., 2020). For the HRDEM, oceans have been converted to voids by the Canada Centre for Mapping and Earth Observation (CCMEO).

The 3-second SRTM Digital Elevation Model (DEM) of Australia defined all water bodies from the SRTM Water Body Data and the elevations were set to the same elevations as in the DSM.

Flattening of water bodies is generally straightforward provided water areas are well delineated and the shorelines and land and water interface are well identified. Hydro-flattening is achieved by using a 3D breakline along the shoreline of a water body which establishes elevations of the water surface, and produce an aesthetically acceptable water surface in the DEM (Sagar S. & Alper, 2016). The shoreline of a water body can be defined as the line of contact between land and water. Manual digitization of shorelines

from aerial images is very time-consuming and images alone cannot be used to determine the shorelines in vegetated areas, which present challenges to shoreline definition. In the following, we provide some key automated/semi-automated techniques to conduct this step.

GDEM generated the ASTER Global Water Body Database (ASTWBD) (Abrams et al., 2020) that delineates water bodies and thus enables their correction. Specifically, sea waterbodies were identified using the global sea-waterbody database that was created using GTOPO30. Then, if the sea-waterbody area is larger than 80% of the sea waterbody GTOPO30 database, this area is identified as a sea waterbody (Fujisada et al., 2018). The land–sea interface is determined during ASTER GDEM generation by calculating the ratio of the number of stacked-sea-waterbody data to the total number of stacked-pixel data. If the ratio is larger than 0.5, the pixel is assigned as a part of the sea waterbody. Otherwise, the pixel is land. For high latitudes (presence of sea ice), a sea ice removal process was carried out (Figure 34).

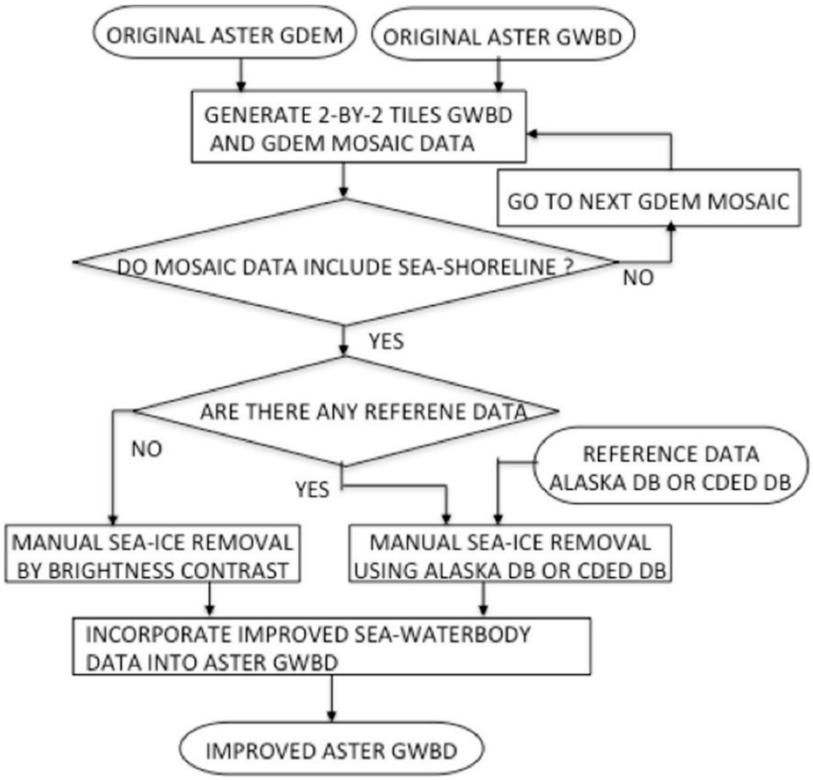

Figure 34. Algorithm for sea ice removal using the global water database (GWBD)

An automated method for 3D breaklines detection is described in Toscano et al. (2013).

Interpolation Strategies for Small Voids

As previously mentioned, the interpolation area should not exceed 16 contiguous pixels to avoid artifacts. If this is not the case, data fusion strategies should be used instead. Interpolating a small void is based on the surrounding valid pixels. Common interpolation algorithms can be divided into local and global approaches. Local techniques predict the value of an unknown point based on the values of neighbourhood pixels whereas global interpolation techniques use all available sample points to generate a prediction for a pixel.

Prominent local interpolation methods include:

- Weighted averaging: the value of a pixel is computed by a weighted average of surrounding pixels. The weights can be computed by:
    - Kriging–a geostatistical interpolation method that utilizes variogram which depends on the spatial distribution of data. However, such an implementation requires specifying a semi-variogram model.
    - Inverse distance–weights are calculated as inverse distances (optionally raised to a power) from the location to be estimated to sampled points in a defined neighbourhood. The inverse distance weighting technique was used for processing WorldDEM small voids (Collins et al., 2015).
- Local polynomial interpolation.
- Nearest neighbour interpolation: finds the closest subset of input samples to a query point and applies weights to the based on proportionate areas (Arun, 2013).
- Radial basis function interpolation.

Global interpolation methods include:

- Spline interpolation: uses a mathematical function to minimize the surface curvature and produces a smooth surface that exactly fits the input points.
- ANUDEM: uses an interpolation technique specifically designed to create a surface that more closely represents a natural drainage surface and preserves both ridgelines as well as stream networks. It has been applied for other larger void areas by the JPL in the processing of SRTM data (Siemonsma, 2015) and for processing Australian DEM (Program, n.d.). It's one of the most suitable approaches for filling of voids and it creates a hydrologically correct DEM (Reuter et al., 2009). ANUDEM approach is implemented in ArcGIS as TOPOGRID.

These interpolation methods are significantly influenced by the terrain characteristics around the voids and tend to generate discontinuous boundaries at joints. In general, Kriging performs better when compared to other contemporary methods in most contexts. Specifically, Kriging has been found to adapt itself to terrain variations, while ANUDEM is found preferable for streams and ridge lines (Arun, 2013). Regarding void size, a linear interpolation technique is better suited for isolated tiny gaps (maximum of 4 pixels), whereas inverse distance weighting interpolation is preferred for voids that are relatively small, dispersed and near water bodies (González et al., 2020).

For the HRDEM, 35% of void areas span less than 1 square kilometers. We think that a large portion of these voids will be cleared in the new version of ArcticDEM. These small voids are located within diverse land cover and elevations. For example, small voids in the north are located within water areas, barren land, lichen-moss cover and snow and ice. They also are mainly located along dissected terrain as shown in Figure 35. Considering this, spline interpolation should be favoured for small and medium sized voids in high altitude and dissected terrain. Kriging or inverse distance weighting interpolation should be used for small- and medium-size voids in relatively flat low-lying areas (Reuter et al., 2007). For larger voids in other terrains, ANUDEM should be used. It should be noted that the CCMEO conducted small void filling for the HRDEM.

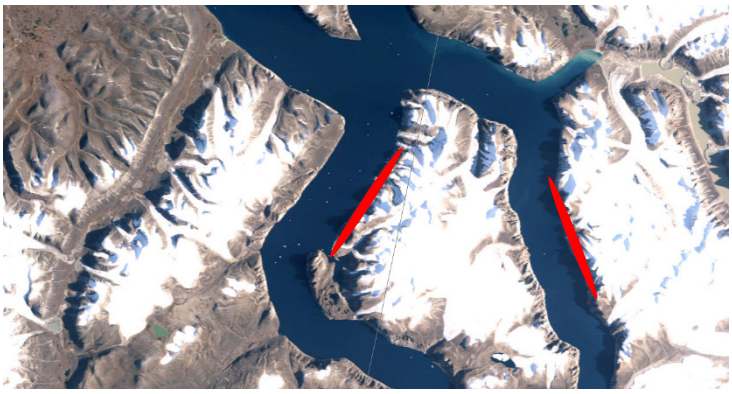

Figure 35. Small voids located within dissected terrain in the HRDEM

Small Artifacts

Small artifacts usually represent outliers and noise in the data. Thus, these interpolation strategies pose a challenge for local outliers' detection. Local outliers can be defined as small, very improbable features which could be just noise in the data collection method. This is very common for remote sensing based instruments (Reuter et al., 2009, p. 4). Detection strategies are often based on statistical approaches like the following:

- Computing the median value for a circular region centred at each pixel of a given radius. If the median value is outside a certain confidence interval, the pixel is considered an outlier. Then a new value is computed by interpolation (Huber et al., 2021).
- Calculating the probability of finding a certain value within the neighbourhood of a pixel by comparing the original elevation with the value estimated from the neighbours. Kriging which is probabilistic statistical interpolation method that can be used to estimate the elevation by considering the spatial structure of the data. Kriging will calculate weight based on distance in the interpolation if sample elevation data. The distances represent the correlation structure among sample points, that is how similar they are with distance and is represented in variogram model. The difference between estimated and true value is calculated for each pixel to derive overall average and standard deviation. Then, assuming a Gaussian distribution, Student's t test can be used to standardize the differences (Hengl et al., 2004).

For HRDEM, the artifacts were manually digitized by CCMEO technicians and only the most obvious and major artifacts were delineated. Consequently, some small data artifacts were not identified. The median value-based outlier detection described above is a reasonably accurate technique and can be implemented within a GIS software. This will require setting some hyperparameters: radius of the circular region and the confidence interval. For interpolation, rules discussed in the previous section should be followed.

Depressions

Depressions may occur in DEMs because of limited horizontal and vertical resolution of elevation data or resulting from the interpolation. Thus, it is very important to deal with these artifacts after conducting the interpolation of small voids. Common algorithms include (Lindsay & Creed, 2005):

- Filling: raises the elevations of cells in the DEM grid. This algorithm is well known and is the most widely used. It has been implemented in most GIS software and tool packages that support digital terrain analysis and hydrological modelling.

- Breaching: lowers cell elevations along a breach channel. This has been implemented in TOPAZ (Topographic Parameterization), a digital terrain analysis software for watershed modelling.
- The physically based erosion model for pit and flat areas removal (PEM4PIT): performs the correction by applying a simplified physically based landscape evolution equation (Fernandez et al., 2016).

Currently, there is still no one algorithm which can satisfactorily deal with depressions in grid DEMs under various application contexts (Wang et al., 2019). However, experiments showed that the TOPAZ method seems to be preferable for correcting depressions in areas of irregular relief as well as flat regions, while PEM4PIT is preferable for correcting depressions located in regions of medium slopes (Fernandez et al., 2016).

As HRDEM is intended for hydrological modelling among other applications, correcting depressions should consider relief information. The breaching technique integrated within the TOPAZ software is favoured for areas of varying terrain as well as flat regions and can be used for HRDEM.

Spikes

Spikes and wells are single pixel elevation errors, where the elevation of a point on the surface model is significantly different from the elevations of its neighbours. A spike is a positive elevation difference, while a well is a negative elevation difference to neighbouring pixels. WorldDEM product (Collins et al., 2015) removed these artifacts with an interpolation using the eight neighbouring pixel elevations. For the development of NASADEM, ASTER Global Elevation Models (GDEM) was used for void filling (Crippen et al., 2016). However, GDEM uses autocorrelation and thus contains topographic spikes and sometimes wells. They propose a method to eliminate spikes and pits with no ancillary data by computing the curvature instead of the slope and then applying spatial filters. For Europe's Copernicus DEM (Airbus, n.d.), spikes and wells were identified using 20 m minimum height difference of centre pixels compared to the average elevation of its eight neighbours and then interpolated using the neighbours.

For simplicity, a spike detection algorithm should be implemented for HRDEM. This could be based on the median value-based outlier detection as it fulfills the same purpose. The identified spikes should be interpolated according to their terrain location as described in section 9.5.1.2.

Furthermore, spikes and wells can also result from interpolation or DEM fusion. Instead of the well-known interpolation techniques described above, some DEMs used other smoothing methods. EarthEnv-dem90 (Robinson et al., 2014) and MERIT DEM (Yamazaki et al., 2017) used an adaptive, multi-scale smoothing technique that was originally proposed by (Gallant, 2011). Regular smoothing tends to impact important surface features obliterating important fine details. The multi-scale smoothing enables an adaptive smoothing depending on the local relief. The source code of this smoothing technique is not available. However, enough details are provided by the authors to enable an implementation from scratch.

Random Errors/Noise

Random errors are often associated with the measurement error, i.e., signal noise. They can be significant for the DEMs produced using remote sensing-based imaging instruments but are inherent in any measurement process. Overcoming noise is made by applying spatial filters. Different types of spatial filters exist (Reuter et al., 2009, p. 4):

- Median filter
- Tension splines

- Fast Fourier Transform MERIT DEM (Yamazaki et al., 2017)
- Wavelet analysis
- Kalman filter

Noise doesn't pose a significant problem for DEMs derived from optical remote sensing instruments as any measurement errors are corrected prior to DEM production. Any remaining errors can be detected and interpolated or smoothed as discussed in the previous sections.

Correction of Absolute Bias in DEMs

The absolute bias can be recognized as a shift in the average elevation over a large domain (typically>20 km scale) in a DEM (Yamazaki et al., 2017). A set of ground elevations points can be used to estimate the difference between two DEM sources. MERIT DEM used ICESat (Ice, Cloud, and land Elevation Satellite) laser altimetry as ground reference (Yamazaki et al., 2017) to detect the absolute bias by calculating the difference between the DEM and ICESat centroid elevations. To estimate the absolute bias, the mean elevation difference between the stripe-noise-removed MERIT DEM and ICESat centroid elevations was calculated for each 1/12° tile. The elevations were assumed to be the same between the MERIT DEM and ICESat centroid if there was no absolute bias where topography is not too steep and tree density is not so high. A detailed account is given in (Yamazaki et al., 2017). Practically, to improve the quality of a DEM using ICESat data, the relationship between ICESat elevations, terrain factors (slope, relief and aspect) and land uses can be simulated using machine learning models (Chen et al., 2020). Improved ICESat-2 data can be used as ground control points to improve the quality of DEMs using a point-to-surface matching algorithm, which is fully automated (Lee and Hahn 2020). In HRDEM, this bias was vastly corrected with ICESat by the Polar Geospatial Center, but this correction was not implemented for the upcoming version 4 of ArcticDEM.

New Technologies for DEM Anomalies Correction

In this section, more sophisticated techniques for DEM anomaly correction are presented.

DEM Fusion

Sparse Representation

Using sparse representations, DEM fusion is represented as a mathematical optimization problem that could be solved to achieve global optimality. In this technique the area of interest is segmented into overlying patches of grid cells. Dictionaries of patches (i.e., unique combinations of terrain shape) are created. Sparse representations allow mitigating one of the weaknesses of a simple weighted averaging, namely that it uses pixels independently (Schindler et al., n.d.).

Frequency Domain Filtering

The frequency domain filter is an established technique proposed for fusion of DEMs, i.e., void filing by data fusion (Karkee et al., 2008). The lower frequency portion of one DEM (i.e., the coarser terrain features) can be isolated and merged with the higher frequency portion of another DEM (i.e., the finer terrain features) of the same area. This has been applied to DEMs generated with InSAR and stereo-photogrammetry techniques since the InSAR DEMs tend to be more accurate in the high frequency, and the stereo-photogrammetric DEMs tend to be more accurate in the low frequencies. This technique involves four main steps: converting the DEMs into the frequency domain; applying a low or high-pass filter to the appropriate DEM; adding the two desired DEM portions; converting the resultant data back to the spatial domain.

k-means Clustering

This technique involves the fusion of multiple, overlapping DEMs. This fusion method is based on the distribution of elevations at each cell location, and the user input is limited to data distribution parameters. The algorithm includes the following steps: slope and elevation thresholding, k-means clustering and adaptive mean and Gaussian filtering (Fuss et al., 2016).

Voids Interpolation

Deep Learning-based Techniques

Deep Neural Networks

Artificial neural networks are nonparametric models that can learn complex and highly nonlinear relationships between any numbers of different variables. They can thus be used to correct nonlinear errors in DEMs. Deep learning is being used more frequently for processing DEM in the last years. This has been applied for SRTM elevations over dense urban areas (Salah, 2021). Because these errors are nonlinear, they cannot be handled by most traditional methods. Practically, the set of features that can be used for prediction are extracted from the RGB and VNIR bands of Sentinel 2 images and SRTM. Namely, the gray level co-occurrence matrix textures, slope and aspect of the DEM can act as good features for training a neural network. Another interesting example is training a neural network to predict the target 1 arcsecond SRTM value from a feature vector. In Kulp and Strauss 2018, the authors used a 23 dimensional vector: the 3x3 window including that pixel in the 1-arcsecond SRTM, the 3x3 window for the 3-arcsecond SRTM, the slope value computed with some technique, the population density and the estimated ICESat error at the target pixel obtained from the 1-degree mean SRTM-ICESAT differential map, canopy height at target pixel and finally vegetation density at target pixel.

Conditional Generative Adversarial Network (CGAN)

Besides discriminative models like deep neural network, deep generative models entail a great potential for DEM generation. For example, (Gavriil et al., 2019 use a deep generative model to construct a complete elevation model without voids with semantically plausible generated values. In Qiu et al. (2019), the voids of a DEM were filled using a deep convolutional generative adversarial network.

Zhu et al. (2020) formalize spatial interpolation as a conditional generative task using a conditional encoder-decoder generative adversarial neural network. They showed that GANs can support the extraction of latent topographic information and reconstruct terrains with consistent topographic characteristics.

COSTING

For confidentiality reasons, this section has been removed from the public version of the report. Only the summary is provided here.

SUMMARY

Other than the new upcoming ArcticDEM data, there is no available high-resolution DEM products in the Arctic within the 2 m resolution and licenses for open access. Correcting anomalies will require a combination of new data collection and vendor products. The viable first tier solutions that can meet the accuracy and resolution specifications consist of the following:

Tier 1–Solutions meeting HRDEM current accuracy and resolution:

- Intermap–Airborne InSAR system
- VeriDaaS–Geiger Mode LiDAR
- Hexagon–Single Photon LiDAR
- NextMap One–2 m Processing (optical imagery)

Other conditional solutions consist of the following:

Tier 2–Conditional solutions:

- AW3D Enhanced–2 m Processing (optical imagery may have licensing issues)
- Radarsat-2–3 m Process (SAR radargrammetry, limitation is surface time and coarse resolution)

NextMap One provides a viable solution for producing data elevation data over selected land cover. Depending on availability of operational facility and collection requirements, Geiger Mode LiDAR, Single Photon LiDAR and airborne InSAR are suitable technologies to collect data over various terrains in the Arctic. In forested areas, Geiger Mode LiDAR and Single-Photon LiDAR would be best suited for data collect.

RECOMMENDATIONS

In summary, these are our recommendations on the next steps:

1. It is anticipated that by the end of 2022, a new version of the ArcticDEM will be released (version 4). This version utilizes a median-based blending strategy that will make use of all valid pixels in previously discarded strips. Consequently, we believe this will decrease the total area of voids present in the ArcticDEM. It is expected that both a reduction of data artifacts and voids will occur. It is recommended that no correction or data collection be conducted until ArcticDEM version 4 is made available. A detailed comparative analysis is recommended to be conducted to quantify both the improvement and remaining deficiencies. Nonetheless, as our strip analysis showed, we believe that a minimum of 2,661 km^2 of voids will still be present after the integration. These results are preliminary and thus we recommend conducting a new data anomaly analysis after the integration.

2. Automated methodologies for detecting anomalies should be investigated and developed to create a comprehensive list of defects by location. We recommend using a local outlier detection strategy to uncover data artifacts. The most straightforward solution is a radius based median filter. Machine learning can also be used by training a model to estimate a pixel's elevation from its neighbours. The identified outliers will be set to anomalies as voids.

3. Afterwards, we recommend stratifying the anomalies based on their area or a number of pixels and grouping them into size categories. For example, very small anomalies (smaller than 16 pixels), small anomalies (smaller than 1 km^2) and big anomalies (bigger than 1 km^2). A classification strategy can be used to determine the intervals (natural breaks, standard deviation, etc.). Then, we recommend aggregating these anomalies into different terrain units based on slope and altitude. This will enable to determine which terrain unit contains which anomaly classes. Based on this organization, we recommend spline interpolation for small and medium sized anomalies in high altitude and cliffs, in combination with Kriging, or inverse distance weighting for small and medium sized anomalies for relatively flat-lying areas. For large voids over lowlands, a TIN or ANUDEM interpolation is recommended.

4. The remaining anomalies determined by the detection methods should be then organized and prioritized based on size, location, landcover and cluster density (proximity to concentration of anomalies). Next, it should include priorities based on needs such as water studies, geological activities, and/or infrastructure projects. The needs should be jointly decided with CCMEO, Territories and Provinces based on location of improvements and cost-sharing. A multi-criteria analysis approach using the Delphi and Analytical Hierarchy Process is a possible method to facilitate identification of priority areas.

5. No off-the-shelf DSM is available at the resolution and accuracy desired for HRDEM and that can be licensed for open public use in the Canadian Arctic. A level of collection and processing will be required to address the remaining data anomalies. Based on needs and anomaly analysis conducted new data will be required. New data collection is to be driven by costs and likelihood of successful collection. ArcticDEM illustrated that land cover of glacial features, lichen-moss, forest and water are least favourable for satellite stereo-imagery.

6. Establish an ongoing semi-annual review of elevation and mapping data needs across the HRDEM geography to discuss collaborative priorities for collection and addressing data anomalies with Federal, Provincial and Territorial governments.

7. We also recommend investigating deep learning-based models for DEM void filling. These models can learn from medium resolution DEMs and other auxiliary information like slope and land cover to produce a high-resolution DEM. An even more promising class of techniques are generative models (GANs) that can learn to produce a high-resolution DEM from a low resolution one (super-resolution). Appropriately implementing such a model can minimize data acquisition requirements.

REFERENCES

Abdelfattah, R., & Nicolas, J. M. (2002). Topographic SAR interferometry formulation for high-precision DEM generation. IEEE Transactions on geoscience and remote sensing, 40(11), 2415–2426.

Abrams, M., Crippen, R., & Fujisada, H. (2020). ASTER Global Digital Elevation Model (GDEM) and ASTER Global Water Body Dataset (ASTWBD). *Remote Sensing*, *12*(7), 1156. https://doi.org/10.3390/rs12071156

Airbus (2018). WorldDEM, Technical Product Description, version 2.4.

Airbus (2021). WorldDEM Neo, Technical Product Description, version 1.0.

Airbus (n.d.). Pléiades Imagery User Guide.

Airbus (n.d.). Spot Imagery User Guide

Aguilar, M. A., del Mar Saldana, M., & Aguilar, F. J. (2013). Assessing geometric accuracy of the orthorectification process from GeoEye-1 and WorldView-2 panchromatic images. International Journal of Applied Earth Observation and Geoinformation, 21, 427–435.

Arun, P. V. (2013). A comparative analysis of different DEM interpolation methods. *The Egyptian Journal of Remote Sensing and Space Science*, *16*(2), 133–139. https://doi.org/10.1016/j.ejrs.2013.09.001

Berthier, E., Vincent, C., Magnússon, E., Gunnlaugsson, Á. Þ., Pitte, P., Le Meur, E., ... & Wagnon, P. (2014). Glacier topography and elevation changes derived from Pléiades sub-meter stereo images. The Cryosphere, 8(6), 2275–2291.

Baqué, R., Du Plessis, O. R., Castet, N., Fromage, P., Martinot-Lagarde, J., Nouvel, J. F., ... & Martineau, P. (2017, October). SETHI/RAMSES-NG: New performances of the flexible multi-spectral airborne remote sensing research platform. In 2017 European Radar Conference (EURAD) (pp. 191–194). IEEE.

Candela, S. G., Howat, I., Noh, M. J., Porter, C. C., & Morin, P. J. (2017, December). ArcticDEM Validation and Accuracy Assessment. In AGU Fall Meeting Abstracts (Vol. 2017, pp. C51A-0951).

Charbonneau, F. (2021), Canada Centre for Remote Sensing, Personal Communication.

Chen, C., Yang, S., & Li, Y. (2020). Accuracy assessment and correction of SRTM DEM using ICESat/GLAS data under data coregistration. Remote sensing, 12(20), 3435.

Clavet, D., Toutin, T., & Kharbouche, E. S. (2011). Radarsat-2: une nouvelle source pour l'acquisition de données topographiques dans l'Arctique Canadien sans contrôle terrain. Canadian Journal of Remote Sensing, 37(5), 529–534.

Collins, J., Riegler, G., Schrader, H., & Tinz, M. (2015). APPLYING TERRAIN AND HYDROLOGICAL EDITING TO TANDEM-X DATA TO CREATE A CONSUMER-READY WORLDDEM PRODUCT. *The International*

Archives of the Photogrammetry, Remote Sensing and Spatial Information Sciences, *XL-7/W3*, 1149–1154. https://doi.org/10.5194/isprsarchives-XL-7-W3-1149-2015

Crippen, R., Buckley, S., Agram, P., Belz, E., Gurrola, E., Hensley, S., Kobrick, M., Lavalle, M., Martin, J., Neumann, M., Nguyen, Q., Rosen, P., Shimada, J., Simard, M., & Tung, W. (2016). NASADEM GLOBAL ELEVATION MODEL: METHODS AND PROGRESS. *ISPRS - International Archives of the Photogrammetry, Remote Sensing and Spatial Information Sciences*, *XLI-B4*, 125–128. https://doi.org/10.5194/isprsarchives-XLI-B4-125-2016

Digital Globe (n.d) - Digital Globe Core Imagery Products Guide" - 2.5 BASIC STEREO PAIR IMAGERY PRODUCTS

Deilami, K., & Hashim, M. (2011). Very high resolution optical satellites for DEM generation: a review. European Journal of Scientific Research, 49(4), 542–554.

Eckert, S., & Hollands, T. (2010). Comparison of automatic DSM generation modules by processing IKONOS stereo data of an urban area. IEEE Journal of Selected Topics in Applied Earth Observations and Remote Sensing, 3(2), 162–167.

Faherty, D., Schumann, G. J. P., & Moller, D. K. (2020). Bare Earth DEM generation for large floodplains using image classification in high-resolution single-pass InSAR. Frontiers in Earth Science, 8, 27.

Farr, T. G., Rosen, P. A., Caro, E., Crippen, R., Duren, R., Hensley, S., Kobrick, M., Paller, M., Rodriguez, E., Roth, L., Seal, D., Shaffer, S., Shimada, J., Umland, J., Werner, M., Oskin, M., Burbank, D., & Alsdorf, D. (2007). The Shuttle Radar Topography Mission. *Reviews of Geophysics*, *45*(2), RG2004. https://doi.org/10.1029/2005RG000183

Fernandez, A., Adamowski, J., & Petroselli, A. (2016). Analysis of the behavior of three digital elevation model correction methods on critical natural scenarios. *Journal of Hydrology: Regional Studies*, *8*, 304–315. https://doi.org/10.1016/j.ejrh.2016.09.009

Fujisada, H., Urai, M., & Iwasaki, A. (2018). Technical Methodology for ASTER Global Water Body Data Base. *Remote Sensing*, *10*(12), 1860. https://doi.org/10.3390/rs10121860

Fuss, C. E. (n.d.). *Digital Elevation Model Generation and Fusion*. 169.

Fuss, C. E., Berg, A. A., & Lindsay, J. B. (2016). DEM Fusion using a modified *k*—means clustering algorithm. *International Journal of Digital Earth*, *9*(12), 1242–1255. https://doi.org/10.1080/17538947.2016.1208685

Gallant, J. (2011). *Adaptive smoothing for noisy DEMs*. 4.

Gavriil, K., Muntingh, G., & Barrowclough, O. J. D. (2019). Void Filling of Digital Elevation Models with Deep Generative Models. *IEEE Geoscience and Remote Sensing Letters*, *16*(10), 1645–1649. https://doi.org/10.1109/LGRS.2019.2902222

Gesch, D., Oimoen, M., Danielson, J., & Meyer, D. (2016). Validation of the ASTER global digital elevation model version 3 over the conterminous United States. The International Archives of Photogrammetry, Remote Sensing and Spatial Information Sciences, 41, 143.

González, C., Bachmann, M., Bueso-Bello, J.-L., Rizzoli, P., & Zink, M. (2020). A Fully Automatic Algorithm for Editing the TanDEM-X Global DEM. *Remote Sensing*, *12*(23), 3961. https://doi.org/10.3390/rs12233961

Hengl, T., Gruber, S., & Shrestha, D. P. (2004). Reduction of errors in digital terrain parameters used in soil-landscape modelling. *International Journal of Applied Earth Observation and Geoinformation*, *5*(2), 97–112. https://doi.org/10.1016/j.jag.2004.01.006

Hoja, D., Reinartz, P., & Schroeder, M. (2007). Comparison of DEM generation and combination methods using high resolution optical stereo imagery and interferometric SAR data. Revue française de photogrammétrie et de télédétection, 2006(4), 89-94.

Hu, F., Gao, X. M., Li, G. Y., & Li, M. (2016). DEM EXTRACTION FROM WORLDVIEW-3 STEREO-IMAGES AND ACCURACY EVALUATION. International Archives of the Photogrammetry, Remote Sensing & Spatial Information Sciences, 41.

Huber, M., Osterkamp, N., Marschalk, U., Tubbesing, R., Wendleder, A., Wessel, B., & Roth, A. (2021). Shaping the Global High-Resolution TanDEM-X Digital Elevation Model. *IEEE Journal of Selected Topics in Applied Earth Observations and Remote Sensing*, *14*, 7198–7212. https://doi.org/10.1109/JSTARS.2021.3095178

Karkee, M., Steward, B. L., & Aziz, S. A. (2008). Improving quality of public domain digital elevation models through data fusion. *Biosystems Engineering*, *101*(3), 293–305. https://doi.org/10.1016/j.biosystemseng.2008.09.010

Kulp, S. A., & Strauss, B. H. (2018). CoastalDEM: A global coastal digital elevation model improved from SRTM using a neural network. *Remote Sensing of Environment*, *206*, 231–239. https://doi.org/10.1016/j.rse.2017.12.026

Lin, Y. C., Shao, J., Shin, S. Y., Saka, Z., Joseph, M., Manish, R., Fei, S., & Habib, A. (2022). Comparative Analysis of Multi-Platform, Multi-Resolution, Multi-Temporal LiDAR Data for Forest Inventory. Remote Sensing, 14(3). https://doi.org/10.3390/rs14030649

Lindsay, J. B., & Creed, I. F. (2005). Removal of artifact depressions from digital elevation models: Towards a minimum impact approach. *Hydrological Processes*, *19*(16), 3113–3126. https://doi.org/10.1002/hyp.5835

Lombardi, N., Lorusso, R., Fasano, L., & Milillo, G. (2016, July). Interferometric COSMO-SkyMed spotlight DEM generation. In 2016 IEEE International Geoscience and Remote Sensing Symposium (IGARSS) (pp. 6495–6498). IEEE.

Luedeling, E., Siebert, S., & Buerkert, A. (2007). Filling the voids in the SRTM elevation model—A TIN-based delta surface approach. *ISPRS Journal of Photogrammetry and Remote Sensing*, *62*(4), 283–294. https://doi.org/10.1016/j.isprsjprs.2007.05.004

Magnard, C., Frioud, M., Small, D., Brehm, T., Essen, H., & Meier, E. (2014). Processing of MEMPHIS Ka-band multibaseline interferometric SAR data: From raw data to digital surface models. IEEE Journal of Selected Topics in Applied Earth Observations and Remote Sensing, 7(7), 2927–2941.

Massonnet, D., & Souyris, J. C. (2008). Imaging with synthetic aperture radar. EPFL press.

Maune, D. (2020). The Challenges and Joys of Mapping America's Last Frontier. Photogrammetric Engineering & Remote Sensing, 86(4), 202–207.

Méric, S., Fayard, F., & Pottier, É. (2009). Radargrammetric SAR image processing. Geoscience and remote sensing, 421–454.

Mercer, B. (2007). National and regional scale DEMs created from airborne INSAR. Proceedings of PIA07—Photogrammetric Image Analysis, 36, 113–118.

Moller, D., Hensley, S., Wu, X., & Rodriguez, E. (2011, December). Millimeter-Wave Airborne Interferometry for High-accuracy Topography Mapping. In AGU Fall Meeting Abstracts (Vol. 2011, pp. G11B-03).

Mulawa, D., Comp, C., & Clarke, B. (2018) Geolocation Accuracy Performance of the DigitalGlobe Constellation during 2017 and 2018 H1, JACIE 2018.

Neuenschwander, A., Guenther, E., White, J. C., Duncanson, L., & Montesano, P. (2020). Validation of ICESat-2 terrain and canopy heights in boreal forests. Remote Sensing of Environment, 251, 112110.

Nikolakopoulos, K. G. (2020). Accuracy assessment of ALOS AW3D30 DSM and comparison to ALOS PRISM DSM created with classical photogrammetric techniques. European Journal of Remote Sensing, 53(sup2), 39–52. https://doi.org/10.1080/22797254.2020.1774424

Nonin, P., Decluseau, D., Gabet, L., & Bernard, M. (2013). 3D capabilities of SPOT 6. Technical Report, 1–20.

Noh, M. J., & Howat, I. M. (2015). Automated stereo-photogrammetric DEM generation at high latitudes: Surface Extraction with TIN-based Search-space Minimization (SETSM) validation and demonstration over glaciated regions. GIScience & remote sensing, 52(2), 198–217.

Ontario Report, 2022. User guide, Ontario Digital Elevation Model (Imagery-Derived), Provincial Mapping Unit.

Papasaika, H., Poli, D., & Baltsavias, E. (2009). Fusion of Digital Elevation Models from Various Data Sources. *2009 International Conference on Advanced Geographic Information Systems & Web Services*, 117–122. https://doi.org/10.1109/GEOWS.2009.22

Papasodoro, C., Royer, A., Langlois, A., & Berthier, E. (2016). Potential of RADARSAT-2 stereo radargrammetry for the generation of glacier DEMs. Journal of Glaciology, 62(233), 486–496. https://doi.org/10.1017/jog.2016.44

Polar Geospatial Center (2022) Personal communication

Program, B. A. (n.d.). *Geoscience Australia, 3 second SRTM Digital Elevation Model (DEM) v01* [Data set]. Retrieved February 11, 2022, from https://data.gov.au/data/dataset/12e0731d-96dd-49cc-aa21-ebfd65a3f67a

Raggam, H., Gutjahr, K., Perko, R., & Schardt, M. (2009). Assessment of the stereo-radargrammetric mapping potential of TerraSAR-X multibeam spotlight data. IEEE Transactions on Geoscience and Remote Sensing, 48(2), 971–977.

Qiu, Yue, & Liu. (2019). Void Filling of Digital Elevation Models with a Terrain Texture Learning Model Based on Generative Adversarial Networks. *Remote Sensing*, *11*(23), 2829. https://doi.org/10.3390/rs11232829

Reuter, H. I., Hengl, T., Gessler, P., & Soille, P. (2009). Chapter 4 Preparation of DEMs for Geomorphometric Analysis. In *Developments in Soil Science* (Vol. 33, pp. 87–120). Elsevier. https://doi.org/10.1016/S0166-2481(08)00004-4Reuter, H. I., Nelson, A., & Jarvis, A. (2007). An evaluation of void-filling interpolation methods for SRTM data. *International Journal of Geographical Information Science*, *21*(9), 983–1008. https://doi.org/10.1080/13658810601169899

Robinson, N., Regetz, J., & Guralnick, R. P. (2014). EarthEnv-DEM90: A nearly-global, void-free, multi-scale smoothed, 90m digital elevation model from fused ASTER and SRTM data. *ISPRS Journal of Photogrammetry and Remote Sensing*, *87*, 57–67. https://doi.org/10.1016/j.isprsjprs.2013.11.002

Sagar S., D., & Alper, Y. (2016). *A semi-automatic method to Hydro-flatten LiDAR data*. Imaging & Geospatial Technology Forum.

Salah, M. (2021). SRTM DEM correction over dense urban areas using inverse probability weighted interpolation and Sentinel-2 multispectral imagery. *Arabian Journal of Geosciences*, *14*(9), 801. https://doi.org/10.1007/s12517-021-07148-6

Saldaña, M. M., Aguilar, M. A., Aguilar, F. J., & Fernández, I. (2012). DSM Extraction and evaluation from geoeye-1 stereo imagery. ISPRS Annals of the Photogrammetry, Remote Sensing and Spatial Information Sciences, 4, 113–118.

Schindler, K., Papasaika-Hanusch, H., Schütz, S., & Baltsavias, E. (n.d.). *Improving Wide-Area DEMs Through Data Fusion—Chances and Limits*. 12.

Schumann, G. J. P., Moller, D. K., & Mentgen, F. (2016). High-accuracy elevation data at large scales from airborne single-pass SAR interferometry. Frontiers in Earth Science, 3, 88.

Sefercik, U. G. (2013). Productivity of TerraSAR-X 3D data in urban areas: A case study in trento. European Journal of Remote Sensing, 46(1), 597–612.

Siemonsma, D. (2015). *The Shuttle Radar Topography Mission (SRTM) Collection User Guide*. 17.

Stoker, J. M., Abdullah, Q. A., Nayegandhi, A., & Winehouse, J. (2016). Evaluation of single photon and Geiger mode lidar for the 3D Elevation Program. Remote Sensing, 8(9), 1–16. https://doi.org/10.3390/rs8090767

Sosa, J. (2019). *Jsosa/delta_surf_method* [Python]. https://github.com/jsosa/delta_surf_method (Original work published 2018)

The Commonwealth Scientific and Industrial Research Organisation. (1997). *Current Biology*, *7*(3), R126. https://doi.org/10.1016/S0960-9822(97)70976-X

Toscano, G. J., Gopalam, U., & Devarajan, V. (2013). A NOVEL METHOD FOR AUTOMATION OF 3D HYDRO BREAK LINE GENERATION FROM LIDAR DATA USING MATLAB. *The International Archives of the Photogrammetry, Remote Sensing and Spatial Information Sciences*, *XL-2/W2*, 99–104. https://doi.org/10.5194/isprsarchives-XL-2-W2-99-2013

Toutin, T., & Gray, L. (2000). State-of-the-art of elevation extraction from satellite SAR data. ISPRS Journal of Photogrammetry and Remote Sensing, 55(1), 13–33.

Toutin, T. (2004). Geometric processing of remote sensing images: models, algorithms and methods. International journal of remote sensing, 25(10), 1893–1924.

Toutin, T., Blondel, E., Clavet, D., & Schmitt, C. (2012). Stereo radargrammetry with Radarsat-2 in the Canadian Arctic. IEEE Transactions on Geoscience and Remote Sensing, 51(5), 2601–2609.

Wang, S., Ren, Z., Wu, C., Lei, Q., Gong, W., Ou, Q., Zhang, H., Ren, G. & Li, C. (2019a). DEM generation from Worldview-2 stereo imagery and vertical accuracy assessment for its application in active tectonics. Geomorphology, 336, 107–118.

Wang, Y.-J., Qin, C.-Z., & Zhu, A.-X. (2019b). Review on algorithms of dealing with depressions in grid DEM. *Annals of GIS*, *25*(2), 83–97. https://doi.org/10.1080/19475683.2019.1604571

Wang, H., Zhu, J., Fu, H., & Yu, Y. (2021). Refining the conversion between phase and height in airborne and UAV

Watanabe, K., Sefercik, U. G., Schunert, A., & Soergel, U. (2011). Evaluation of INSAR DEM from high-resolution spaceborne SAR data. In International Archives of the Photogrammetry, Remote Sensing and Spatial Information Sciences: [ISPRS Hannover Workshop 2011: High-Resolution Earth Imaging for Geospatial Information] 38-4 (2011), Nr. W19 (Vol. 38, No. W19, pp. 359–364). Göttingen: Copernicus GmbH.

White Joanne C., Penner Margaret, and Woods Murray. Assessing single photon LiDAR for operational implementation of an enhanced forest inventory in diverse mixedwood forests. The Forestry Chronicle. 97(01): 78–96. https://doi.org/10.5558/tfc2021-009

Yamazaki, D., Ikeshima, D., Tawatari, R., Yamaguchi, T., O'Loughlin, F., Neal, J. C., Sampson, C. C., Kanae, S., & Bates, P. D. (2017). A high-accuracy map of global terrain elevations. *Geophysical Research Letters*, *44*(11), 5844–5853. https://doi.org/10.1002/2017GL072874

Yu, J. H., Li, X., Ge, L., & Chang, H. C. (2010). Radargrammetry and interferometry SAR for DEM generation. In 15th Australasian Remote Sensing & Photogrammetry Conf. Alice Springs, Australia (pp. 1212–1223).

Zhu, D., Cheng, X., Zhang, F., Yao, X., Gao, Y., & Liu, Y. (2020). Spatial interpolation using conditional generative adversarial neural networks. *International Journal of Geographical Information Science*, *34*(4), 735–758. https://doi.org/10.1080/13658816.2019.1599122

Zhou, Y., Parsons, B., Elliott, J. R., Barisin, I., & Walker, R. T. (2015). Assessing the ability of Pleiades stereo imagery to determine height changes in earthquakes: A case study for the El Mayor-Cucapah epicentral area. Journal of Geophysical Research: Solid Earth, 120(12), 8793–8808.